ORIGINAL PAPER

Rare Earth and Critical Element Chemistry of the Volcanic Ash-fall Parting in the Fire Clay Coal, Eastern Kentucky, USA

Jingjing Liu · Shifeng Dai · Debora Berti · Cortland F. Eble ·
Mengjun Dong · Yan Gao · James C. Hower

Abstract In the search for rare earth and other critical elements in coal measures, the coals are emphasized with lesser consideration for the accompanying rocks. In this investigation, the focus is on a lanthanide-rich, 315–317 Ma (after Machlus et al., *Chemical Geology*, *539*, art. no. 119485, 2020) volcanic ash-fall trachyandesite to trachyte tonstein which occurs in association with the Middle Pennsylvanian Duckmantian-age Fire Clay coal in eastern Kentucky. The tonstein was deposited largely during peat accumulation, although it is known to occur at the base of the coal or within the underclay. The mineralogy is dominated by kaolinite with illite and quartz as minor to major minerals. A number of accessory minerals, as detected by X-ray diffraction + Siroquant XRD software and scanning and transmission electron microscopy (S/TEM), include REE-bearing phosphates (apatite, crandallite, florencite, monazite), and Y-bearing zircon. The highest rare earth element + Y concentrations occur in the weathered tonsteins, probably due to the concentration of these minerals after weathering of kaolinite from the rock.

Keywords Critical elements · Lanthanides · Sustainability · Tuffaceous deposits

J. Liu
School of Resources and Geosciences, China University of Mining and Technology, Xuzhou, China
e-mail: liujingjing_cumtb@outlook.com

S. Dai · M. Dong · Y. Gao
College of Geoscience and Survey Engineering, China University of Mining and Technology (Beijing), Beijing 100083, China
e-mail: daishifeng@gmail.com

M. Dong
e-mail: dongmengjundmj@qq.com

Y. Gao
e-mail: gaoyan6gaoyan@126.com

D. Berti
Department of Oceanography, Texas A&M University, College Station, TX 77843–3146, USA
e-mail: deborasm74@runbox.com

C. F. Eble
Kentucky Geological Survey, University of Kentucky, Lexington, KY 40506, USA
e-mail: eble@uky.edu

J. C. Hower (✉)
Center for Applied Energy Research, University of Kentucky, 2540 Research Park Drive, Lexington, KY 40511, USA
e-mail: james.hower@uky.edu

J. C. Hower
Department of Earth & Environmental Sciences, University of Kentucky, Lexington, KY 40506, USA

⊘ Springer

Introduction

Altered volcanic ash beds within coal seams are referred to as tonsteins; they occur mainly as thin and laterally persistent bands in coal. As with organic matter, tonsteins are significant components of coal, from both academic and practical perspectives. They may provide useful information on: the depositional environments, diagenetic and epigenetic processes within coal beds, and coal-bearing strata; geologic events, in this case related to a volcanic eruption; coal-basin formation; and regional tectonic evolution (Arbuzov et al., 2023; Zhang et al., 2022, 2023). Tonsteins may contain minerals (such as zircon and sanidine) suitable for radiometric age determination (Dai et al., 2017c; Nechaev et al., 2022). Practically, tonsteins can be used as chronostratigraphic markers to identify and correlate coal beds during coal exploration and exploitation. Alkali tonsteins may contain critical elements (e.g. rare earth elements (REE) and Y, Nb, Zr, Ga), and thus have the potential as raw materials for the recovery of these critical metals (Dai et al., 2017c; Hou et al., 2023; Jiu et al., 2023; Karayigit et al., 2021; Liu et al, 2021; Shen et al., 2021; Sutcu et al., 2021). Tonsteins can also affect the quality of mined coals through elevating the mineral matter content; this can be a source of abrasion, agglomeration, corrosion, or pollution associated with coal use (Davis et al., 2021; Ward, 2016). With the exception of the Devonian, tonsteins occur widely in sequences representing almost all coal-forming ages, including the Pennsylvanian, Permian, Late Triassic, Jurassic, Late Cretaceous, Paleocene, and Neogene. Tonsteins have been found in numerous coals on all continents and in ranks ranging from lignite, through various bituminous coals, to anthracite.

The Middle Pennsylvanian Duckmantian-age Fire Clay coal, one of the most important coal resources in the Central Appalachians, contains a lanthanide-rich volcanic-ash fall tonstein. This tonstein, dated at 315--317 Ma (Machlus et al., 2020), contributes to the coal's reputation as one of the premier coal-based REE resources in the world (Seredin & Dai, 2012; after Mardon & Hower, 2004). In most cases within this study area, the ash was deposited during the peat accumulation (Andrews et al., 1994; Bohor & Triplehorn, 1981; Chesnut, 1985; Eble et al., 1994; Greb et al., 1999, 2002; Hower et al., 1994, 1999, 2016, 2018, 2020, 2022; Lyons et al., 1992, 2006; Mardon & Hower, 2004). Not all the ash fall is found as a megascopic rock. At the Mardon and Hower (2004) and Hower et al. (2018) site to the west of this study area, the ash is mixed with the macerals within the coal. In a few cases, the tonstein is found at the base of the coal or within the underclay (Eble et al., 1994; Hower et al., 1994).

Aspects of the chemistry and petrology of the coal and tonstein were discussed by Robl and Bland (1977), Bohor and Triplehorn (1981), Hower et al. (1994, 1999,
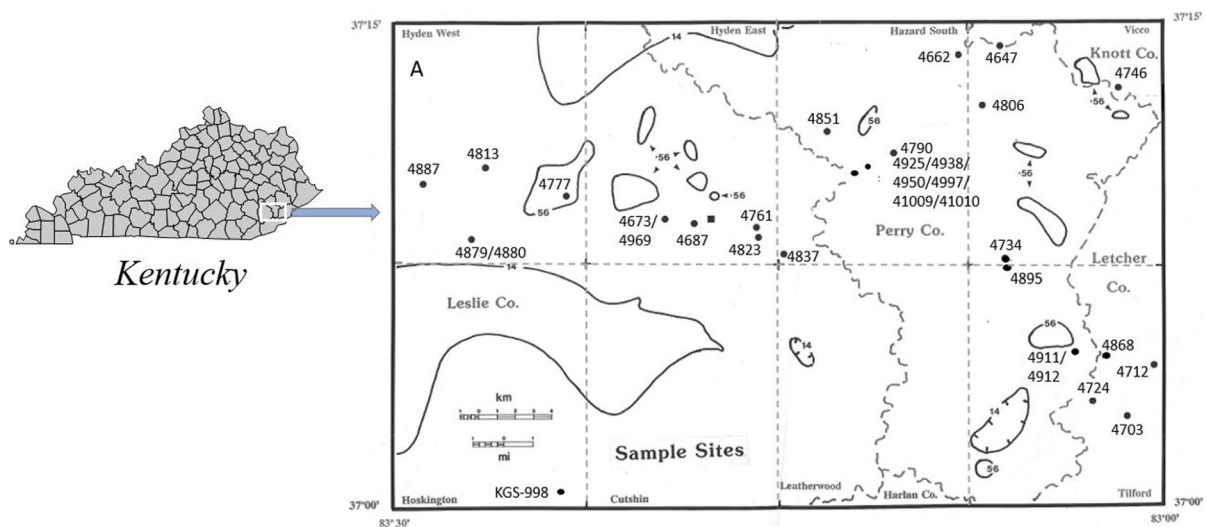

Fig. 1 Locations of the tonstein and other sample sites within central eastern Kentucky, USA

2016, 2020), and Hower et al. (2022) and will not be discussed in detail here. While the earlier studies established the nature of the tonstein, they did not have the advantage of modern analytical techniques such as inductively coupled plasma mass spectrometry (ICP-MS). The present study is based on the suite of samples collected by Hower and Eble and others (at least one of the Hower and Eble team was part of every sampling crew) in 1990 through early 1992. The tonstein, while not the sole target of the comprehensive coal + rock sampling, was appreciated to be a unique part of the

coal seam and, therefore, was always sampled during the field campaign. The purpose of the present study was to carry out mineralogical and geochemical analyses to characterize the enrichment in REE, Y, and other critical elements in the Fire Clay tonstein.

Samples and Methods

Samples were collected by Hower, Eble, and colleagues from 1990 through 1992, with all but one

Table 1 Sample, sample type, location (7½' quadrangle, county, north latitude, west longitude), thickness (cm) for samples analyzed in the present study

Sample	Type	Quadrangle	County	N Lat	W Long	Thick
						(cm)
4647	tonstein	Vicco	Knott	37.23585	83.10149	16.00
4662	tonstein	Hazard South	Perry	37.23166	83.12741	7.87
4673	tonstein	Hyden East	Leslie	37.14911	83.32207	28.96
4687	tonstein	Hyden East	Leslie	37.13857	83.30367	18.80
4703	floor	Tilford	Letcher	37.0466	83.02287	
4712	tonstein	Tilford	Letcher	37.07253	83.00702	13.97
4724	tonstein	Tilford	Letcher	37.05509	83.04731	10.92
4734	tonstein	Vicco	Perry	37.12972	83.10194	11.43
4746	tonstein	Vicco	Knott	37.21444	83.02778	8.38
4761	tonstein	Hyden East	Leslie	37.14472	83.25917	12.45
4777	tonstein	Hyden West	Leslie	37.16056	83.39028	10.92
4790	tonstein	Hazard South	Perry	37.18417	83.17056	9.14
4806	tonstein	Vicco	Perry	37.20806	83.1175	10.49
4813	tonstein	Hyden West	Leslie	37.175	83.44028	7.59
4823	tonstein	Hyden East	Leslie	37.13833	83.26417	12.19
4837	tonstein	Hazard South	Leslie	37.13167	83.24694	9.09
4851	tonstein	Hazard South	Perry	37.19508	83.21501	9.50
4868	floor	Tilford	Letcher	37.08111	83.03778	
4879	tonstein	Hyden West	Leslie	37.13694	83.44639	8.00
4880	floor	Hyden West	Leslie	37.13694	83.44639	2.01
4887	tonstein	Hyden West	Leslie	37.16389	83.48319	11.51
4895	tonstein	Vicco	Perry	37.12722	83.09806	10.49
4911	tonstein	Tilford	Perry	37.08056	83.05417	2.49
4912	floor	Tilford	Perry	37.08056	83.05417	3.99
4925	tonstein	Hazard South	Perry	37.18351	83.19198	14.50
4938	tonstein	Hazard South	Perry	37.18236	83.19266	8.51
4950	tonstein	Hazard South	Perry	37.18191	83.19281	13.00
4962	tonstein	Hindman	Knott	37.34278	82.98444	1.50
4969	tonstein	Hyden East	Leslie	37.14911	83.32207	
4997	tonstein	Hazard South	Perry	37.184	83.19169	13.97
41009	tonstein	Hazard South	Perry	37.1808	83.19356	12.19
41010	coal	Hazard South	Perry	37.1808	83.1936	7.62
KGS 998	tonstein	Hoskinton	Leslie	37.0091	83.3922	

KGS Kentucky Geological Survey

Blue type is used for the floor samples and gray type is used for the coal sample

site within the region shown in Fig. 1. One sample, KGS-998, was collected prior to the latter sampling campaign. The samples were collected from counties including Knott, Perry, Leslie, and Letcher, and included 27 tonstein samples, three floor samples, and one coal sample. The samples were preserved in plastic jars at the Kentucky Geological Survey's Earth Analysis and Research Laboratory (EARL) in Lexington, Kentucky. The sample number, type, location, and thickness are presented in Table 1 and Fig. 1. One sample not in the eight-quadrangle area shown in Fig. 1 (sample 4962) is from the Hindman 7½′ quadrangle, northeast of the Vicco 7½′ quadrangle mapped in Fig. 1.

The proximate and total sulfur analyses were conducted at the University of Kentucky Center for Applied Energy Research (CAER) after ASTM procedures (currently ASTM, 2017, 2018a, b). The major oxide analyses attributed to the CAER were performed following Hower and Bland's (1989) procedures on an X-ray fluorescence (XRF) instrument in place at that time. The major oxide analyses attributed to the China University of Mining & Technology (CUMT) were analyzed with a scanning wavelength dispersive X-ray fluorescence spectrometer (XRF; Thermo ARL Advant'XP$^+$, ThermoFisher, Waltham, Massachusetts, USA).

The concentrations of trace elements in the tonsteins, floor, and coal samples were determined by ICP-MS (ThermoFisher, X series II). Before the ICP-MS analysis, the samples were prepared in the following procedure: 50 mg of coal and non-coal samples were digested in a Milestone UltraClave Microwave High Pressure Reactor microwave digestion system (Milestone, Inc., Sorisole, Italy); tonstein and floor samples were digested with 2 mL of HNO$_3$ (65%) and 5 mL of HF (40%); ashed coal samples were digested with 5 mL of HNO$_3$ (65%) and 2 mL of HF (40%). More details of the ICP-MS analysis method were described by Dai et al. (2011).

The mineral phases and their contents in samples were determined by X-ray diffraction (XRD) using a Rigaku D/max-2500/PC X-ray powder diffractometer (Rigaku, Tokyo, Japan), along with the commercial software *Siroquant*™ (Michell, ACT, Australia) developed by Taylor (1991) based on the whole-pattern analysis principles proposed by Rietveld (1969). More details of XRD and *Siroquant* analyses were given by Ward et al. (2001). Each coal sample was subjected to low-temperature ashing (<120°C) using a plasma low-temperature asher (EMITECH K1050X; Quorum, East Sussex, UK) to remove the organic matter prior to XRD analysis.
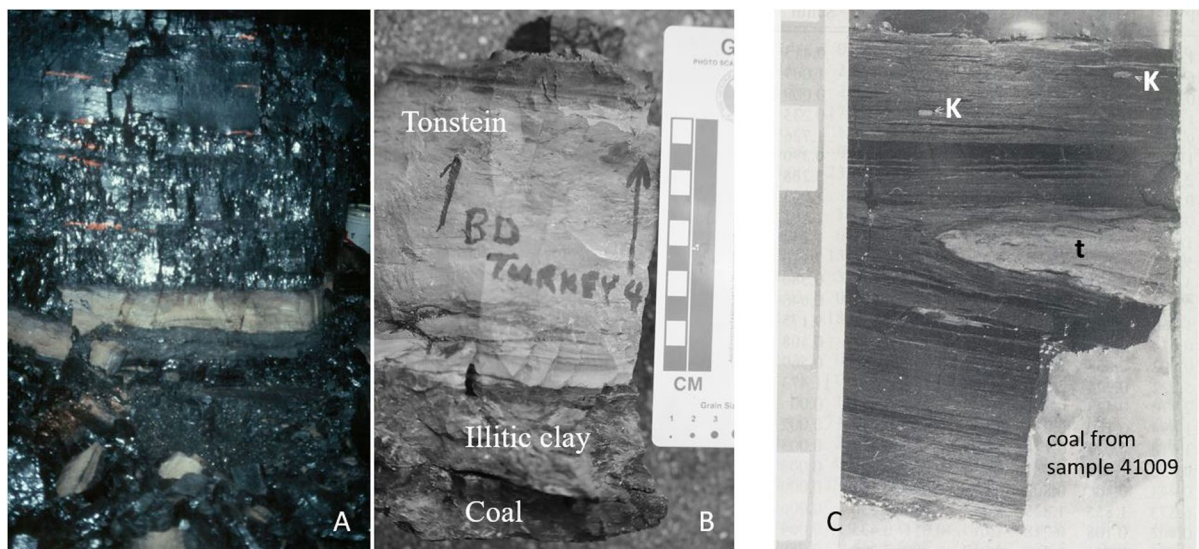

Fig. 2 a Lithologic profile of a coal seam surrounding tonstein sample 4712. **b** Hand specimen of tonstein (sample 4712), the underlying illitic clay (sample 4713 in Hower et al., 1999), and a portion of the lowermost lithotype of the coal (sample 4714 in Hower et al., 1999). Note centimeter scale to the right of hand specimen. **c** Polished block corresponding to coal sample 41010. The coal encases kaolinite lenses (K) and a thin tonstein lens (t). The tonstein was present at the top of the polished coal section. Note centimeter scale to the left of polished block

The morphology and some elemental compositions of minerals in tonsteins were analyzed using a field emission-scanning electron microscope (FE-SEM, FEI Quattro S; ThermoFisher, Waltham, Massachusetts, USA) in conjunction with an energy-dispersive X-ray spectrometer (EDS, Octa-neElect, Berwyn, PA, USA). Samples were carbon-coated using a Quorum Q150T ES (Quorum, East

Table 2 Mineral percentages as determined by XRD and Siroquant (%)

Sample	Type	Kaolinite	Illite	Quartz	Clinoptilolite	Siderite	Rutile	Pyrite	Gypsum	Chlorite	Anatase
4647	tonstein	60.4	34.3	3.8	1.6						
4662	tonstein	74.7	24.0	1.3							
4673	tonstein	39.1	55.5	2.9		2.5					
4687	tonstein	63	32.9	1.2			0.7	2.2			
4703	*floor*	18.5	68.9	12.6							
4712	tonstein	64.3	30	0.4					2.7	2.3	0.3
4724	tonstein	70.6	26.2	3.2							
4734	tonstein	61.8	38.2								
4746	tonstein	65.2	34.1	0.7							
4761	tonstein	70.4	28.7	0.8							
4777	tonstein	67.5	23.8	8.7							
4790	tonstein	69.7	30	0.3							
4806	tonstein	72.3	26	1.7							
4813	tonstein	64.4	35.3	0.3							
4823	tonstein	91.7	6.5	1.7							
4837	tonstein	67.1	32.3	0.6							
4851	tonstein	75.4	24.2	0.4							
4868	*floor*	51.1	42.7	6.2							
4879	tonstein	59	19.7	18.9			2.3				
4880	*floor*	11.7	67.9	14.3						6.2	
4887	tonstein	70.8	29.2								
4895	tonstein	68	31.6	0.3							
4911	tonstein	34.1	44.1	21.9							
4912	*floor*	40.1	43.7	16.2							
4925	tonstein	68.9	30.6	0.5							
4938	tonstein	75.4	24.6								
4950	tonstein	70.8	29.1	0.1							
4962	tonstein	6.3	85	8.7							
4969	tonstein	45	53	2							
4997	tonstein	68.2	31.8								
41009	tonstein	70.8	28.9	0.3							
41010	***coal***	59	38.2	2.8							
KGS 998		69.6	29	1.4							

Tonsteins in regular type, floor rocks in blue italics, and coal in bold blue italics

KGS Kentucky Geological Survey

Sussex, UK) sputter coater. The images of SEM were captured via a retractable solid-state backscatter electron detector. The working distance of the FE-SEM–EDS was ~10 mm, the beam voltage was 20 kV, the aperture was 6, and spot size was 5.0.

Transmission electron microscopy (TEM) images and selected area diffraction patterns (SAED) of the Dean coal sample were collected using a JEOL JEM-2100 (JEOL USA, Peabody, Massachusetts, USA) operated at 200 keV, at the Virginia Tech National Center for Earth and Environmental Nanotechnology Infrastructure (NanoEarth).

Results and Discussion

Mineralogy

As discussed by Robl and Bland (1977), Rice et al. (1994), and Hower et al. (1994), the tonstein (Fig. 2) mineralogy is dominated by kaolinite with lesser amounts of quartz, K-feldspar, illite, and other minerals (Table 2). The Al_2O_3-SiO_2-K_2O chemistry (Fig. 3) supports the dominance of kaolinite, with most samples clustering along the Al_2O_3–SiO_2 axis.

As a caveat concerning the samples, Frank Dulong (Hower et al., 1994; based on a 1991 personal communication with Cortland Eble) noted that sample 4911 might have been transitional to the underclay (sample 4912) resulting in a diminished kaolinite content in the "tonstein" and a relatively high kaolinite content in the underclay. Of the other tonstein samples with <50% kaolinite, 4673 was noted as darkening upwards, perhaps an indicator of an increasing illite content in that part of the rock; 4962 was a parting from a roadcut in the Hindman 7½' quadrangle, thus relatively distant from the other sites; and 4969 was from a weathered roadcut. Basically, the field identification was imperfect and roadcut samples with ~10–15 y of weathering (at the time of the sampling) are imperfect. In this case, the XRD analysis is the final arbiter of the sample type. Setting aside these four gradational (4673 and 4911) and weathered (4962 and 4969) samples, the kaolinite content of the tonstein samples ranges from 59 to >91%. The coal sample included among these samples (41010) contains several flint clay inclusions.

Previous electron microscopy studies include the SEM and high-resolution TEM (HRTEM) investigation of the minerals in a high-REE portion of the Dean coal (a Fire Clay coal correlative) in Knox
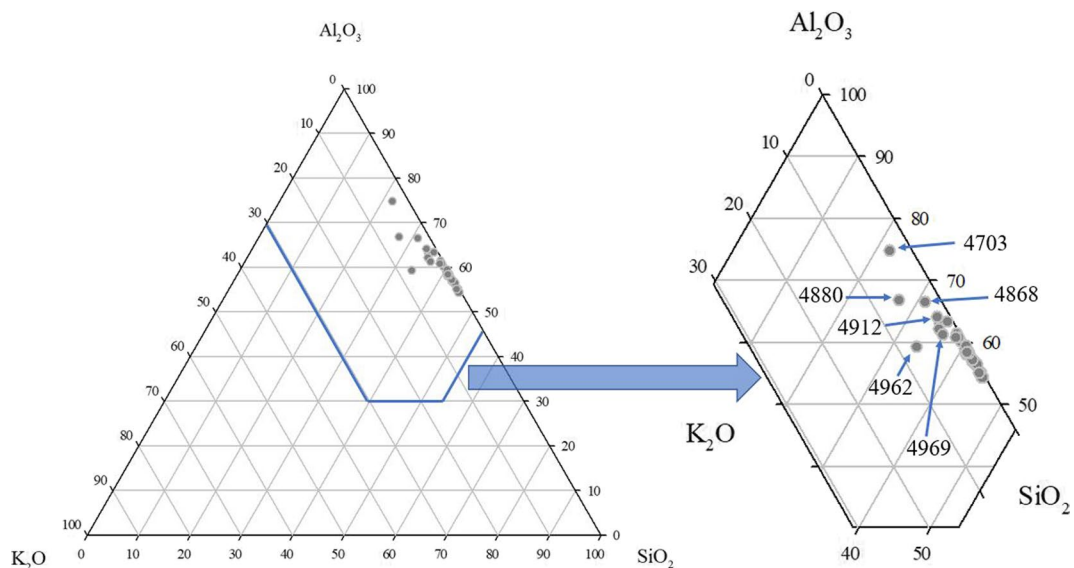

Fig. 3 Al_2O_3–SiO_2–K_2O chemistry of the rock and coal samples. The floor samples (4703, 4898, 4880, and 4912) and the weathered tonsteins (4962 and 4969) are identified

County, Kentucky (Hower et al., 2018; based on samples from Mardon & Hower, 2004). Figure 4a shows interlayered monazite and kaolinite. In this case, the kaolinite could represent the diagenetic recrystallization of the volcanic glass. A well crystallized kaolinite, possibly a phenocryst from the volcanic-ash fall, is shown in Fig. 4b,c. The Dean coal site is different from the sites in the current study in that it has no megascopic tonstein. The lower portion of the coal bed does show an enrichment in REE and does contain abundant kaolinite and trace amounts of monazite, however (Hower et al., 2018).

In addition to minerals identified by XRD, some trace minerals with contents below the detection limits of XRD analysis were identified by SEM–EDS, including K-feldspar and apatite (Fig. 5); zircon (Fig. 6); Ti oxides (rutile or anatase) (Fig. 7); ilmenite, pyrite, crandallite, florencite, and galena (Fig. 8); and siderite and goethite (Fig. 9). Compared to the trace minerals found in the present study, Weaver (1963), in his review of heavy minerals in bentonites, noted that hornblende, biotite, zircon, apatite, and titanite were the most common non-opaque heavy minerals in felsic ashes.
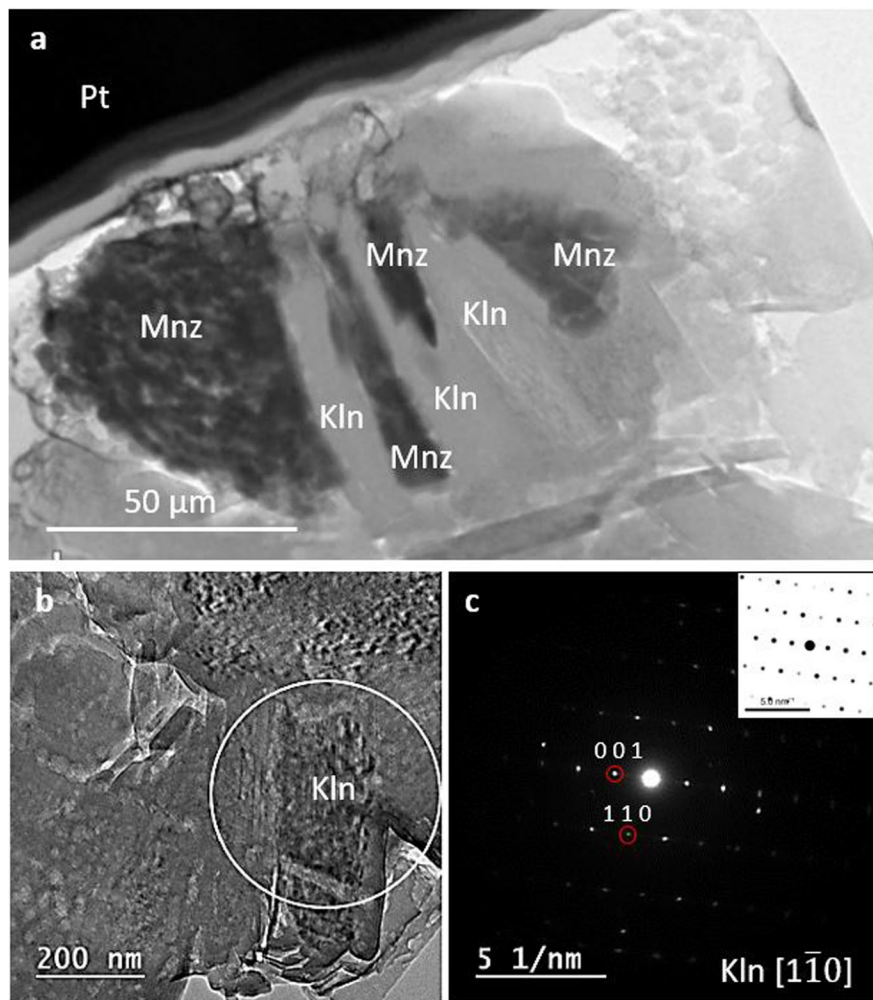

Fig. 4 TEM images of the FIB section. **a** Monazite (mz) and kaolinite (Kln); the black ribbon is a platinum (Pt) protective layer placed on the surface of the sample; **b** kaolinite; **c** selected area electron diffraction pattern (SAED) of the region within the white circle in **b**. The pattern symmetry and d spacing correspond to kaolinite viewed along $[1\bar{1}0]$. The inset shows the kinematic simulation computed with the software *SingleCrystal*®4, using the kaolinite structure by Bish and Von Dreele (1989) which confirms the identification (from Hower et al., 2018)

As indicated by XRD analysis, kaolinite is the main constituent of tonsteins present in this study. In addition to occurring as matrix for other trace minerals, it occurs in vermicular form (Figs. 5a and 7a), indicating an authigenic origin. Vermicular kaolinite is usually considered as evidence of volcanic ash deposition of the partings with coal seams (Dai et al., 2017c), mainly because vermicular kaolinite in the partings is indicative of in situ alteration of volcanic minerals, as reported by Triplehorn and Bohor (1981), Ward (20022016), and Dai et al. (2017c).

The volcanogenic minerals identified in altered volcanic ash layers present in this study that survived post-depositional alteration include mainly sanidine,

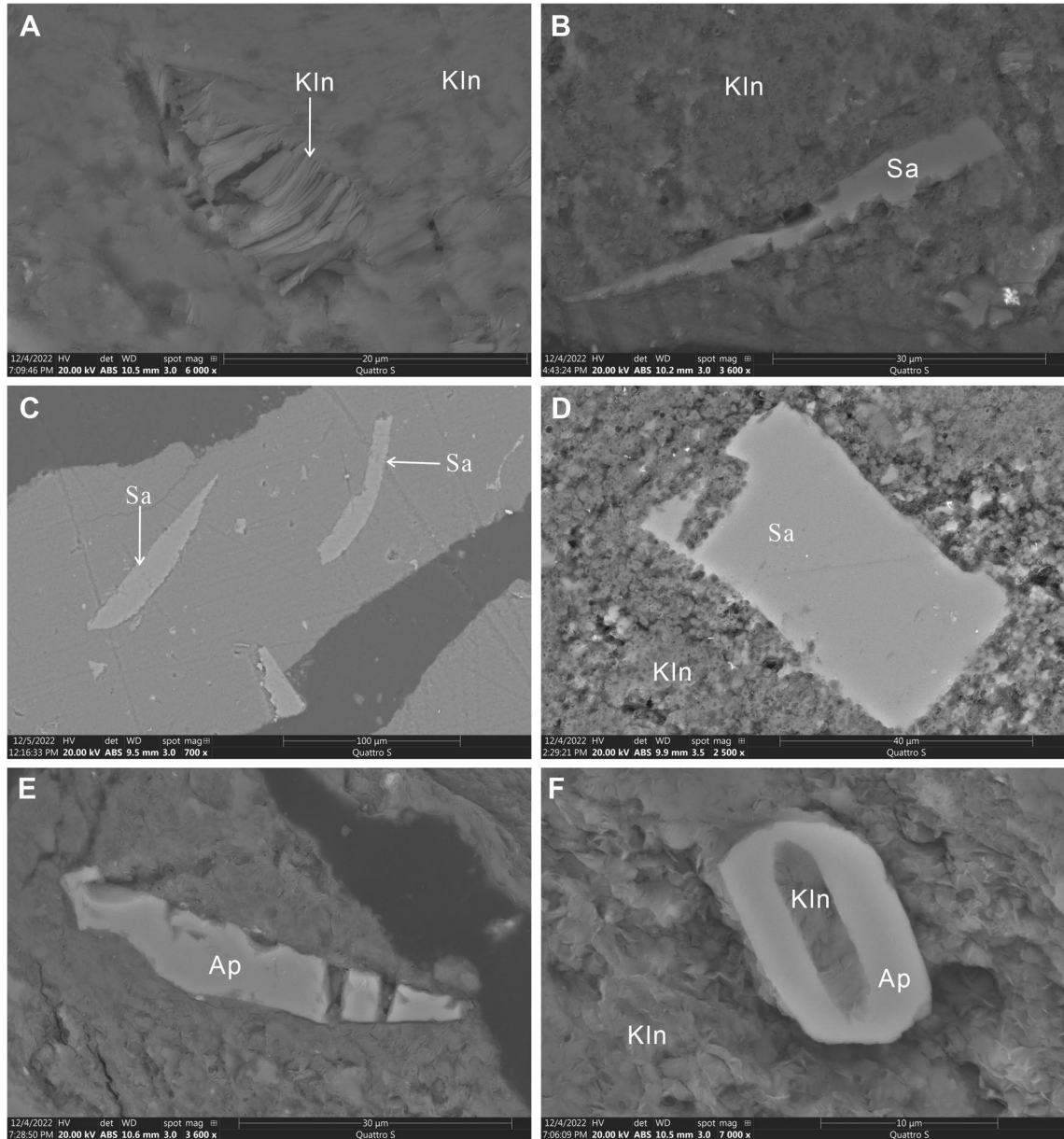**Fig. 5** SEM back-scattered electron images of kaolinite, sanidine, and apatite in tonstein samples: **a** vermicular kaolinite and a matrix kaolinite in sample 4673; **b** sanidine in a kaolinite matrix in sample 4673; **c** sanidine in a kaolinite matrix in sample 4777; **d** sanidine in a kaolinite matrix in sample 4673; **e** and **f** apatite in a kaolinite matrix. Key: Kln, kaolinite; Sa, sanidine; Ap, apatite

zircon, apatite, and rutile (or anatase). Sanidine occurs mainly as anhedral, elongate shards distributed in the kaolinite matrix (Fig. 5b,c). Sanidines shown in Fig. 5b,c have well defined shard-like morphologies strongly suggestive of original subhedral to euhedral sanidine micro crystals being torn apart during an explosive volcanic eruption. Some sanidines are in the form of embayed, tabular euhedral crystals (Fig. 5d). The presence of sanidine supports strongly the volcanic-ash origin of the partings. Apatite occurs typically as individual shard-like grains within a kaolinite matrix (Figs. 5e,f and 8a) and the apatite in a few cases is resorbed, all suggesting a volcanic origin (Fig. 5f). The delicate and elongate apatite grains may have fractured as a result of the volcanic explosion or compaction after deposition (Figs. 5c–e and 8a) (Dai et al., 2017c; Spears, 2012).

In many cases, zircon grains observed in samples that were subjected to SEM–EDS analysis do not show well crystallized shapes, but euhedral crystals are observed (Fig. 6a,b,c). The embayments seen in Fig. 6b,c are evidence of magmatic corrosion. The
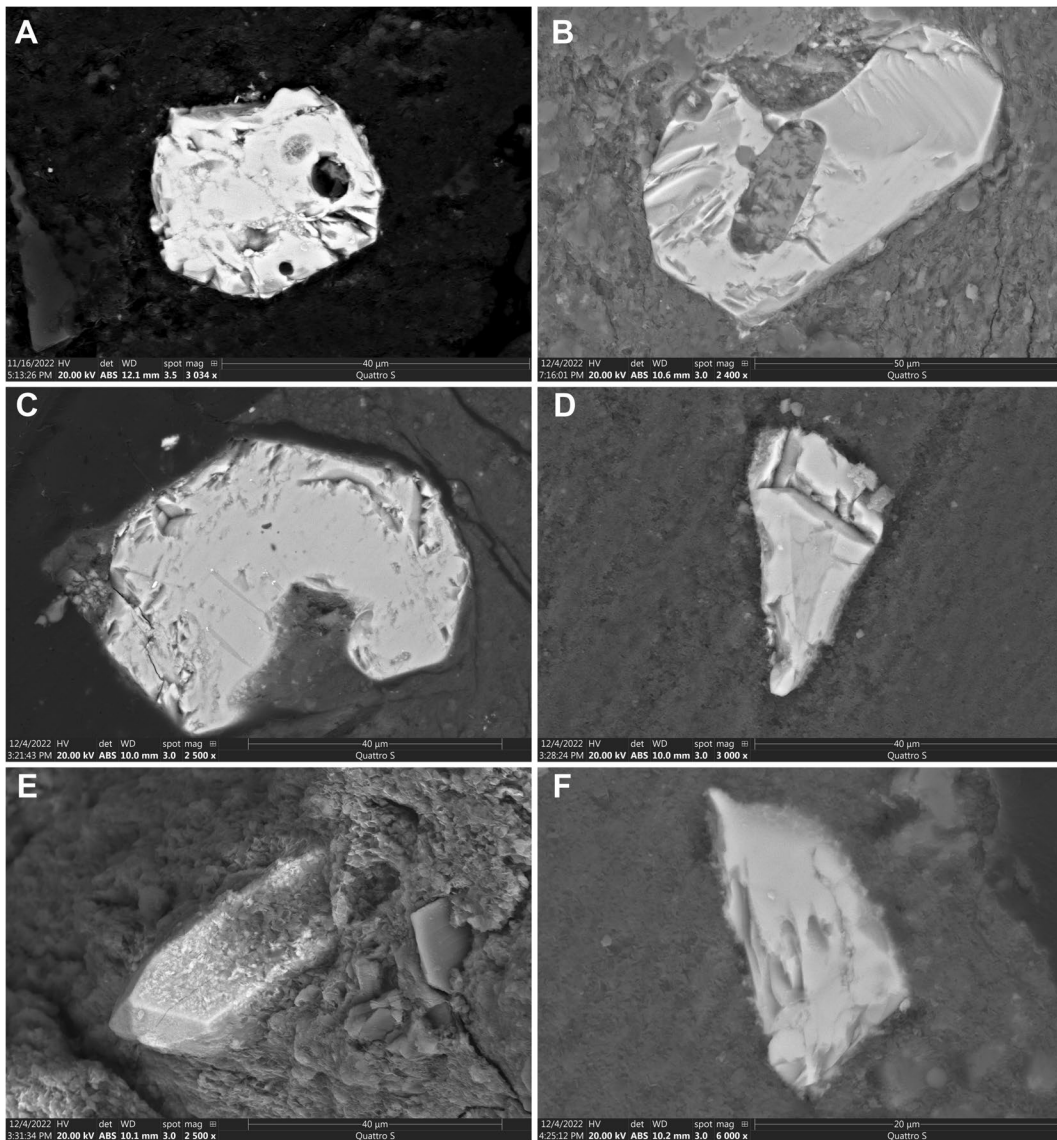

Fig. 6 SEM back-scattered electron images of zircon in sample 4673

zircon grains shown in Fig. 6d,f are clearly fragments of zircon crystals from an explosive volcanic primary origin while the grain shown in Fig. 6e is a euhedral prismatic crystal with well developed terminations. The fractures shown in Fig. 6d,f are probably the result of this explosive volcanic activity which would have shattered original primary subhedral to euhedral zircon micro-crystals. A single tonstein horizon was suggested by Dopita and Kralik (1977) to have an homogeneous population of euhedral zircons with a limited range of shapes. The various shapes of zircon are probably due to modification resulting from the volcanic eruption and transport in the ash cloud. Larger and rounded zircon grains appear to be older than the normal zircon population (Guerra-Sommer et al., 2008), suggesting that the xenocrysts represent partially resorbed older zircons in the magma (Spears, 2012). In addition, some zircon grains contain inclusions (Fig. 6a,b).

Various TiO_2 forms are shown in Fig. 7. Ti oxides in Fig. 7a,b are clearly of authigenic origin, in places (Fig. 7a) clearly intergrown with kaolinite along its cleavage planes. Ti oxides shown in Fig. 7c,d are probably originally magmatic in origin (from the same source as sanidine and zircon grains) and similarly deposited from an explosive volcanic eruption. They would have been primary magmatic Fe-Ti oxides, probably titaniferous magnetite with a well-developed trellis or lattice structure (probably originally magmatic exsolution of Ti oxide in magnetite) and during diagenesis, the Fe was leached out selectively and the Ti oxides have remained behind and now may be the phase 'leucoxene'.

Ilmenite, observed as a partially corroded grain in kaolinite (Fig. 8b), is a resistate volcanogenic mineral and has also been found in a few tonsteins (Bohor & Triplehorn, 1993; Dai et al., 2017c; Lyons et al., 1994). As with apatite, goyazite-gorceixite-crandallite-florencite minerals are often indicative

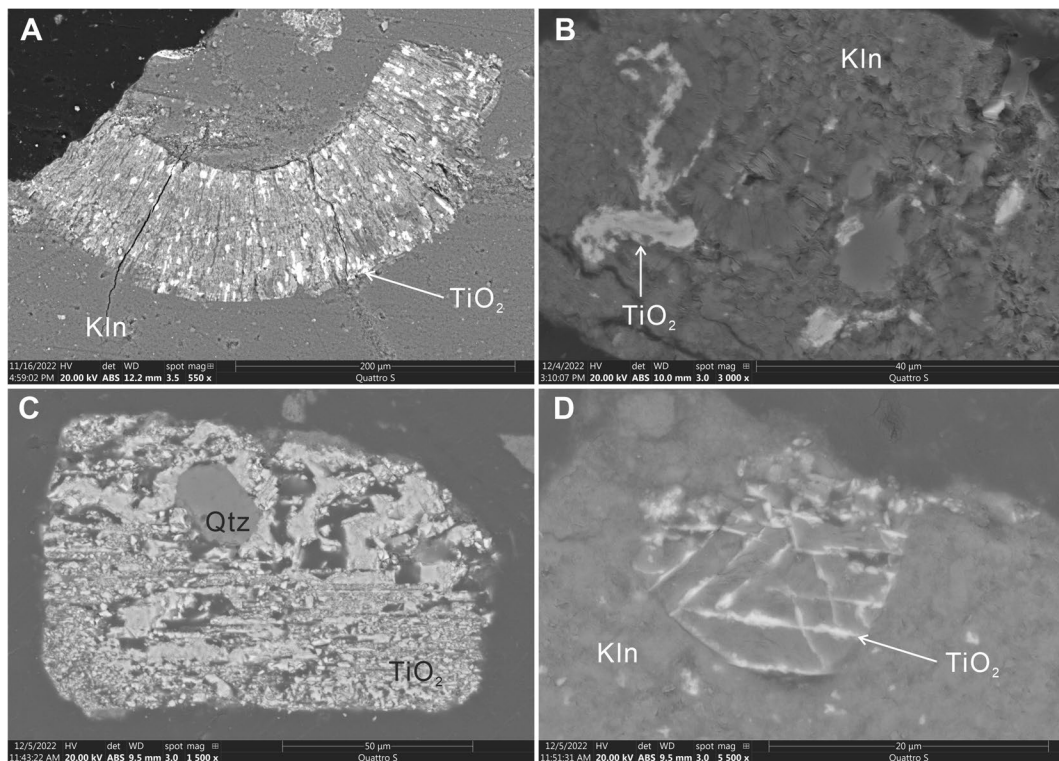**Fig. 7** SEM back-scattered electron images of Ti oxides (rutile or anatase): **a** Ti oxide distributed in vermicular kaolinite in sample 4673; **b** authigenic Ti oxide distributed in a kaolinite matrix in sample 4673; **c** Ti oxides subjected to corrosion and filled with authigenic quartz in sample 4777; **d** Ti oxides subjected to corrosion and filled with kaolinite in sample 4777. Key: Kln, kaolinite; Qtz, quartz

of volcanic input (Brownfield et al., 2005; Dai et al., 2017c; Rao & Walsh, 1997; Wilson et al., 1966; Zhao et al., 2012;) and have been found in a number of tonsteins in coals (e.g. Bohor & Triplehorn, 1993; Kokowska-Pawłowska & Nowak, 2013; Rao & Walsh, 1997). Crandallite and florencite were also identified in tonstein samples present in this study. They occur as individual (Fig. 8c) or as elongated grains (Fig. 8d) in kaolinite.

Sulfide minerals such as pyrite (Fig. 8c) and galena (Fig. 8f) have been observed in the samples present in this study and indicate an epithermal solution input. The pyrite seen in Fig. 8e is of syngenetic or authigenic origin. Siderite has been found in tonsteins, but if present, it is probably of secondary origin (Dai et al., 2017c). Siderite in sample 4763 distributed in kaolinite was subjected to alteration (Fig. 9). Goethite in sample

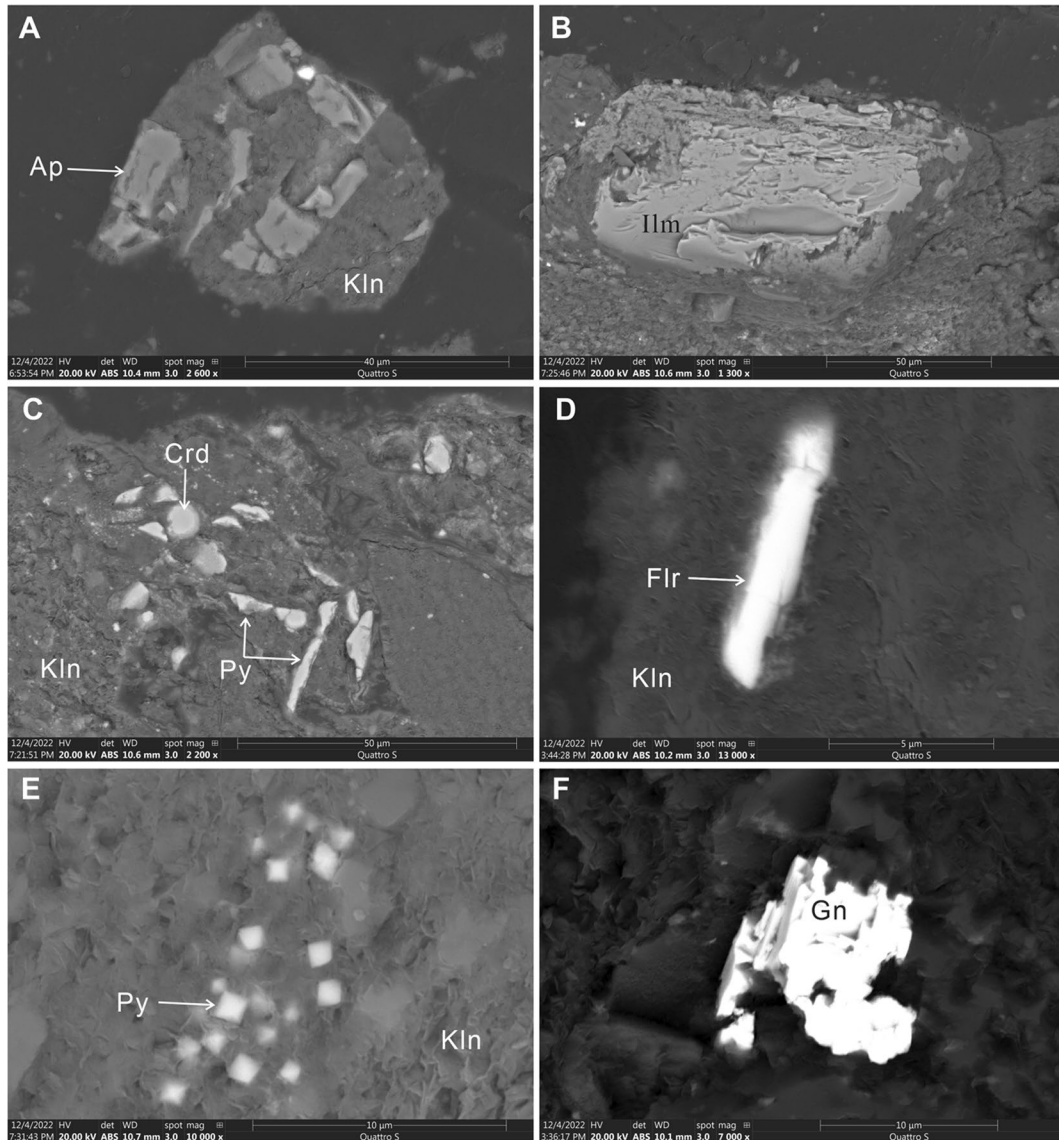**Fig. 8** SEM back-scattered electron images of trace minerals in sample 4673: **a** apatite distributed in a kaolinite matrix; **b** ilmenite in kaolinite; **c** crandallite and pyrite in kaolinite; **d** florencite in kaolinite; **e** euhedral pyrite in kaolinite; **f** galena. Key: Kln, kaolinite; Ap, apatite; Ilm, ilmenite; Crd, crandallite; Flr, florencite; Py, pyrite; Gn, galena

🌀 Springer

4673 (Fig. 9d) with a bell-emulsion shape shows an authigenic origin, possibly as a pseudomorph after siderite because of the rhombohedral shape of the original siderite.

Geochemistry

The chemical analyses of the tonstein, floor rock, and coal are shown in Tables 3, 4, 5, 6, 7, and 8. Both the CAER and CUMT major oxides results are given. The CAER major oxides data were used in the plotting of the figures.

Major Oxides

The major-element oxides in all samples are dominated by SiO_2 and Al_2O_3 (Table 3) with traces of TiO_2, Fe_2O_3, MgO, CaO, MnO, Na_2O, K_2O, and P_2O_5. Among the tonsteins, the amounts of each major element oxide in the two data sets based on CUMT and CAER analyses (Table 3) are very close

to each other. The data for major-element oxides are also consistent with the mineral components in the samples as presented in Table 2. Samples with large illite contents also have large K_2O contents.

Rare Earth Elements

In the present study, REE were used to describe the lanthanide elements, REY for REE + Y, and REYSc for REY + Sc with light REE (LREE) defined as La through Sm and the heavy REE (HREE) defined as Eu through Lu (Hower et al., 1999; Seredin, 1996). Following the normalization of REE abundances to the Upper Continental Crust (UCC) averages (indicated by the subscript suffix 'N') (after Taylor & McLennan, 1985), L-type (light type: $La_N/Lu_N > 1$), M-type (medium type: $La_N/Sm_N < 1$, $Gd_N/Lu_N > 1$), and H-type (heavy type: $La_N/Lu_N < 1$) enrichment patterns are delineated (Seredin & Dai, 2012). Building upon the UCC corrections (Taylor & McLennan, 1985), Ce, Eu, and Gd are decoupled from the other
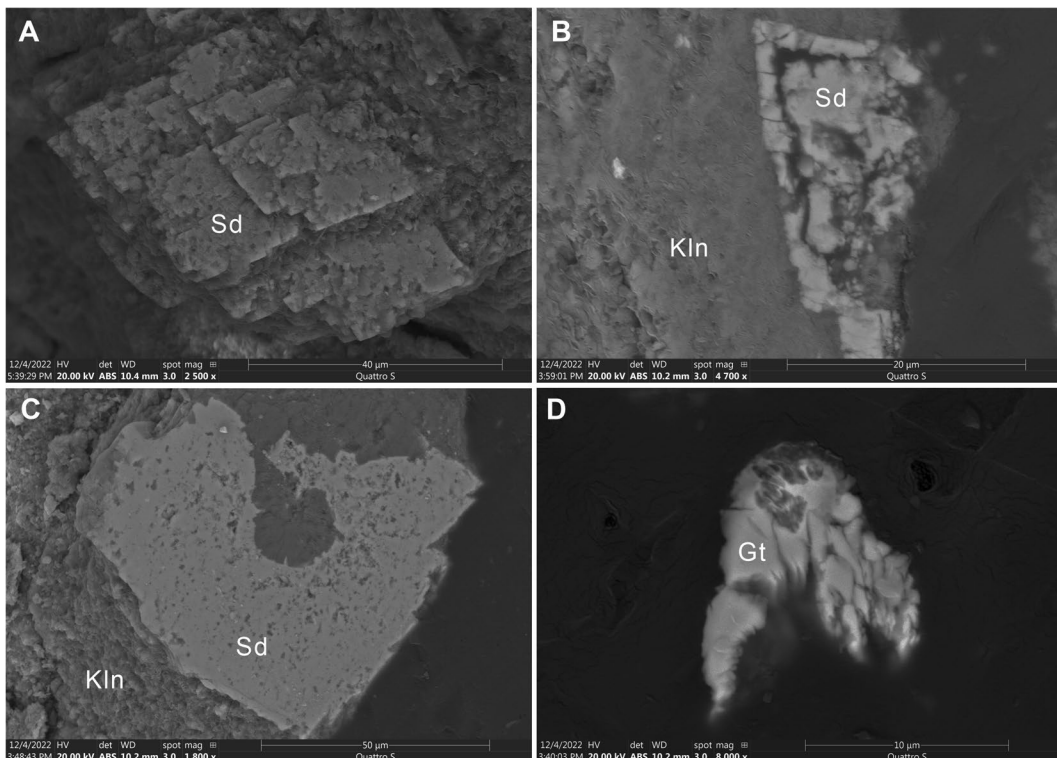

Fig. 9 SEM back-scattered electron images of siderite and goethite in sample 4673: **a** well crystallized siderite; **b** and **c** siderite subjected to corrosion; **d** goethite with a bell-emulsion shape. Key: Sd, siderite; Kln, kaolinite; Gt, goethite

Table 3 **a** Sample; as-determined moisture, ash, and total S; ash-basis major oxides determined at CAER. **b** Sample, ash-basis (%) major oxides determined at CUMT

a

Sample	As-determined basis			CAER XRF (ash basis)									
	Mois	Ash	S_T	Na_2O	MgO	Al_2O_3	SiO_2	P_2O_5	SO_3	K_2O	CaO	TiO_2	Fe_2O_3
4647	1.79	67.06	0.15	0.21	0.15	38.62	54.81	0.11	0.00	0.79	0.23	1.68	1.79
4662	2.42	72.25	0.09	0.31	0.08	43.09	53.13	0.08	0.00	0.34	0.23	1.70	1.86
4673	3.81	84.49	0.05	0.64	1.03	31.80	57.31	0.14	0.04	1.83	0.59	0.92	3.73
4687	3.09	81.76	0.07	0.13	0.08	39.50	55.73	0.08	0.00	0.38	0.44	1.35	0.70
4703	*0.84*	*89.27*	*0.06*	*0.53*	*0.46*	*21.08*	*71.51*	*0.05*	*0.00*	*3.04*	*0.20*	*1.51*	*1.61*
4712	2.91	83.14	0.07	0.09	0.11	40.71	54.41	0.17	0.00	0.40	0.71	1.43	0.91
4724	2.46	83.85	1.62	0.37	0.15	39.98	52.31	0.15	0.00	0.35	0.49	1.25	3.04
4734	2.86	78.78	0.08	0.16	0.08	40.93	54.02	0.05	0.00	0.31	0.47	1.44	0.93
4746	2.46	81.20	0.05	0.09	0.14	40.82	54.27	0.04	0.00	0.20	0.56	1.59	1.03
4761	3.54	83.85	0.04	0.52	0.32	37.93	55.24	0.15	0.00	0.54	0.47	1.44	1.49
4777	2.85	83.08	0.03	0.25	0.11	40.87	54.59	0.12	0.00	0.26	0.42	1.46	0.38
4790	2.66	82.82	0.09	0.68	0.08	39.67	55.24	0.11	0.00	0.34	0.36	1.47	0.64
4806	1.96	74.84	0.14	0.46	0.10	40.41	54.88	0.07	0.00	0.39	0.21	1.94	1.11
4813	2.40	85.67	0.02	0.09	0.08	41.51	53.86	0.05	0.00	0.14	0.30	1.61	0.83
4823	3.10	82.50	0.21	0.17	0.32	38.08	53.53	0.12	0.00	0.42	0.70	1.17	1.19
4837	2.86	82.60	0.80	0.20	0.13	36.65	56.15	0.11	0.00	0.48	0.56	1.27	2.13
4851	2.12	83.77	0.03	0.19	0.11	40.47	54.51	0.09	0.00	0.32	0.46	1.41	0.76
4868	*1.46*	*90.11*	*0.05*	*0.52*	*0.52*	*29.51*	*63.09*	*0.08*	*0.00*	*2.32*	*0.33*	*0.91*	*1.79*
4879	2.78	85.32	0.03	0.15	0.14	34.95	61.99	0.06	0.00	0.81	0.42	1.34	0.73
4880	*0.97*	*94.91*	*0.10*	*0.96*	*1.31*	*24.44*	*59.63*	*0.07*	*0.00*	*5.27*	*0.21*	*0.96*	*4.02*
4887	2.60	84.51	0.11	0.04	0.08	38.49	56.83	0.17	0.03	0.17	0.48	1.42	1.12
4895	2.46	81.55	0.08	0.34	0.08	39.16	55.20	0.08	0.03	0.28	0.36	1.44	1.05
4911	2.27	81.67	0.25	0.29	0.69	32.84	57.82	0.07	0.00	2.40	0.30	1.03	2.58
4912	*1.65*	*89.54*	*0.05*	*0.40*	*0.58*	*31.80*	*60.09*	*0.05*	*0.00*	*1.78*	*0.27*	*1.02*	*2.05*
4925	3.08	80.79	0.09	0.05	0.00	44.63	53.60	0.10		0.43	0.43	1.37	0.32
4938	2.68	83.23	0.32	0.00	0.00	42.45	52.75	0.10		0.42	0.38	1.55	1.08
4950	2.57	83.36	0.08	0.09	0.08	39.07	55.67	0.12		0.49	0.36	1.29	0.91
4962				0.28	1.21	31.50	55.71	0.07		6.63	0.35	1.65	2.60
4969	4.90	84.93	0.02	0.31	1.13	33.65	56.70	0.12	0.03	2.31	0.55	0.83	2.54
4997	3.46	80.58	0.07	0.14	0.12	36.20	58.30	0.10	0.04	0.47	0.50	1.35	0.84
41009	2.58	82.74	0.07	0.16	0.00	36.84	57.80	0.13	0.00	0.44	0.46	1.55	0.70
41010	*2.50*	*16.96*	*0.77*	*0.00*	*0.13*	*35.87*	*57.00*	*0.17*	*0.25*	*0.85*	*0.86*	*1.21*	*1.97*
KGS 998	3.05	85.48	0.10										

REE in the distribution patterns (Bau & Dulski, 1996; Dai et al., 2016b, 2017a, b):

$$Eu_N/Eu_N *= Eu_N/(0.67Sm_N + 0.33Tb_N) \quad (1)$$

$$Ce_N/Ce_N *= Ce_N/(0.5La_N + 0.5Pr_N) \quad (2)$$

$$Gd_N/Gd_N *= Gd_N/(0.33Sm_N + 0.67Tb_N) \quad (3)$$

In addition to the tuffaceous, detrital, infiltrational/leaching, and hydrothermal modes of REE enrichment in coals (Seredin & Dai, 2012), peat and low-rank coals would have had organic associations, with HREE having a greater affinity for organics than the LREE (Aide & Aide, 2012; Davranche et al., 2011; Eskenazy et al., 1986; Eskenazy, 1978, 1987a, b, c, 1999, 2015; Pédrot et al., 2010). As the chelating functional groups diminish in importance in

Table 3 (continued)

b

CUMT XRF (ash basis)

Sample	Na$_2$O	MgO	Al$_2$O$_3$	SiO$_2$	P$_2$O$_5$	SO3	K$_2$O	CaO	MnO	TiO$_2$	Fe$_2$O$_3$
4647	0.15	0.39	30.01	38.59	0.030	0.41	0.83	0.47	0.01	0.98	1.53
4662	0.19	0.24	34.42	37.86	0.023	0.36	0.37	0.48	0.01	0.95	1.41
4673	0.70	1.54	29.48	49.55	0.042	0.07	2.02	0.95	0.02	0.49	2.79
4687	0.09	0.37	39.15	41.34	0.023	0.23	0.38	0.75	0.00	0.88	0.65
4703	*0.48*	*0.80*	*22.40*	*57.92*	*0.013*	*0.08*	*3.44*	*0.38*	*0.01*	*0.86*	*1.40*
4712	0.08	0.47	39.79	41.85	0.054	0.12	0.39	1.04	0.01	0.88	0.68
4724	0.40	0.37	38.99	41.98	0.044	0.88	0.34	0.89	0.01	0.73	2.02
4734	0.12	0.33	38.34	40.10	0.013	0.21	0.29	0.74	0.01	0.82	0.67
4746	0.10	0.46	38.86	40.59	0.012	0.21	0.27	0.82	0.00	1.00	0.83
4761	0.53	0.64	38.22	43.59	0.042	0.08	0.53	0.72	0.00	0.80	0.94
4777	0.07	0.33	41.53	41.64	0.048	0.09	0.28	0.72	0.01	1.17	0.37
4790	0.32	0.23	39.98	40.85	0.028	0.13	0.32	0.64	0.01	0.89	0.53
4806	0.20	0.24	34.96	39.58	0.018	0.31	0.45	0.44	0.01	1.19	0.81
4813	0.06	0.28	41.62	41.53	0.018	0.06	0.19	0.63	0.01	1.10	1.12
4823	0.15	0.68	37.76	42.55	0.030	0.21	0.41	0.98	0.01	0.68	0.89
4837	0.13	0.40	36.20	40.02	0.029	0.57	0.46	0.88	0.00	0.76	1.31
4851	0.12	0.26	39.25	40.51	0.023	0.12	0.33	0.72	0.01	0.84	0.62
4868	*0.34*	*1.08*	*32.52*	*48.78*	*0.021*	*0.04*	*2.45*	*0.60*	*0.01*	*0.53*	*1.51*
4879	0.15	0.49	39.03	43.02	0.015	0.08	0.85	0.67	0.01	0.76	0.63
4880	*0.80*	*1.40*	*23.21*	*53.66*	*0.017*	*0.01*	*5.47*	*0.42*	*0.03*	*0.53*	*3.51*
4887	0.08	0.27	40.12	41.12	0.048	0.19	0.37	0.76	0.02	0.82	0.88
4895	0.27	0.21	37.62	39.27	0.025	0.24	0.29	0.65	0.01	0.88	0.82
4911	0.20	1.01	31.51	45.05	0.017	0.33	2.39	0.59	0.02	0.57	2.15
4912	*0.35*	*1.05*	*34.36*	*47.63*	*0.012*	*0.02*	*1.86*	*0.54*	*0.02*	*0.56*	*1.72*
4925	0.37	0.20	38.82	40.05	0.027	0.22	0.39	0.54	0.00	0.77	0.36
4938	0.33	0.24	39.89	41.04	0.031	0.26	0.36	0.62	0.01	0.88	0.70
4950	0.40	0.36	39.12	41.62	0.039	0.13	0.46	0.58	0.00	0.74	0.72
4962	0.38	0.94	23.62	45.85	0.021	0.36	6.19	0.47	0.01	0.86	2.30
4969	0.67	1.66	30.50	48.86	0.036	0.05	2.23	0.80	0.01	0.45	2.09
4997	0.41	0.37	37.96	40.66	0.028	0.19	0.41	0.64	0.01	0.79	0.73
41009	0.39	0.29	40.10	41.86	0.035	0.13	0.38	0.61	0.00	0.85	0.60
41010	***0.36***	***0.50***	***32.63***	***49.13***	***0.280***	***0.87***	***1.02***	***1.02***	***0.02***	***1.35***	***2.15***
KGS 998	0.07	0.39	39.69	42.21	0.073	0.17	0.36	0.67	0.01	0.84	1.53

KGS Kentucky Geological Survey

Tonsteins in regular type, floor rocks in blue italics, and coal in bold blue italics

bituminous coals (Given, 1984; Hatcher & Clifford, 1996), organic associations are lost from the coal with low LREE/HREE being a ghost signature of the original organic association (Hower et al., 2020). The formerly organic-bound REE could be leached from the coals, bound to clays (Eskenazy, 1995, 1999; Seredin, 1996), or incorporated in secondary carbonates and phosphates. Leaching of LREE from intra-seam and bordering rocks (Dai et al., 2006, 2008) and hydrothermal mobilization of HREE-depleted phosphates and HREE- and Y-enriched organic compounds (Dai et al., 2013a, b, 2016a) contribute to the redistribution of light and heavy REEs. According to Williams-Jones et al. (2012), hydrothermal-influenced deposits tend to be enriched in LREE.

The UCC-normalized REE for all of the samples are shown in Figs. 10 and 11. As noted above, several of the highlighted samples are complicated, being weathered tonsteins (sample 4673 with a distinct negative Eu anomaly; samples 4962 and 4969 do not have a distinct Ce anomaly), floor rock (sample 4703 without a distinct Ce anomaly; sample 4880 with a distinct Ce anomaly), gradational between the tonstein and the floor rock (4911 without a distinct Ce anomaly), or a coal with kaolinite inclusions (41010

Table 4 Sample; ash basis (μg/g) minor elements from Li through Nb; World coal average (ash basis), 2 × World coal average, and 5 × World coal average at bottom of table (after Ketris & Yudovich, 2009).

Sample	Ash basis (μg/g)													
	Li	Be	V	Cr	Co	Ni	Cu	Zn	Ga	Ge	Rb	Sr	Zr	Nb
4647	*250.48*	2.49	58.61	34.02	1.82	12.20	19.90	17.40	30.97	0.94	17.52	37.56	383.29	34.47
4662	*230.39*	2.08	47.74	18.81	1.99	15.73	20.12	13.60	32.82	1.26	6.35	34.37	*469.84*	32.36
4673	63.73	1.17	28.04	34.10	2.75	28.69	26.47	42.40	28.50	0.90	32.72	210.10	371.88	21.31
4687	133.56	1.78	35.03	10.22	1.43	5.82	15.43	31.06	25.51	1.00	2.90	44.54	358.26	32.74
4703	*80.54*	*2.68*	*121.70*	*74.94*	*4.74*	*18.85*	*50.10*	*77.50*	*26.51*	*1.73*	*152.69*	*122.23*	*334.06*	*30.62*
4712	122.48	1.64	38.09	9.66	2.01	4.09	18.41	35.44	24.27	1.05	4.71	39.02	394.06	28.30
4724	122.49	1.11	35.80	8.50	4.78	12.54	19.78	42.99	22.17	0.77	2.95	39.06	412.23	25.79
4734	105.42	0.88	38.41	12.35	1.16	2.58	22.28	28.30	26.73	1.29	3.44	18.18	318.66	34.26
4746	59.50	0.95	39.25	8.36	0.78	1.10	22.64	12.63	26.41	1.49	7.74	15.92	*503.80*	35.31
4761	83.42	0.91	42.39	10.78	5.21	7.28	20.46	49.14	23.49	0.81	3.63	55.22	354.26	29.80
4777	85.25	1.54	33.38	8.35	3.64	5.54	14.44	47.81	25.69	1.03	2.54	5.38	260.22	27.93
4790	129.28	1.27	40.35	10.12	1.06	2.03	19.01	24.10	24.83	1.22	4.80	46.54	389.74	36.52
4806	186.60	2.45	59.51	25.23	2.19	13.31	25.50	25.68	31.07	3.20	9.09	27.68	*495.66*	41.04
4813	89.86	1.24	36.46	9.12	1.91	3.89	18.51	25.20	22.02	1.44	2.61	2.86	395.28	34.26
4823	85.00	0.97	30.58	8.07	3.75	9.24	14.85	46.15	22.75	0.75	1.83	81.25	384.78	27.75
4837	104.20	1.41	37.36	11.09	9.65	19.89	15.51	39.04	23.78	1.03	4.12	75.07	349.16	27.01
4851	106.52	1.26	36.40	9.83	0.66	1.40	12.25	29.88	25.91	1.09	4.14	22.10	336.37	34.38
4868	*77.43*	*5.02*	*54.17*	*29.22*	*1.54*	*6.43*	*19.68*	*31.04*	*25.96*	*1.82*	*41.99*	*35.02*	*279.17*	*29.56*
4879	144.05	5.87	43.96	15.88	1.42	7.33	15.10	23.67	21.72	1.61	11.40	24.21	372.95	35.58
4880	*65.36*	*5.30*	*135.59*	*80.99*	*5.26*	*16.07*	*33.25*	*105.28*	*38.03*	*2.30*	*246.93*	*128.85*	*222.89*	*22.89*
4887	112.12	1.92	41.73	10.71	4.69	7.91	19.33	37.96	21.55	1.21	5.03	9.59	354.66	35.16
4895	97.27	1.01	37.70	11.40	2.21	4.71	18.90	13.74	24.04	1.27	3.22	7.25	445.75	34.91
4911	103.80	5.58	60.67	35.94	5.03	13.72	36.54	34.17	24.88	1.96	48.15	46.15	335.53	24.67
4912	*93.25*	*4.43*	*51.74*	*28.34*	*2.39*	*7.82*	*18.42*	*35.81*	*24.91*	*1.77*	*33.93*	*25.69*	*285.38*	*33.51*
4925	143.31	1.53	32.94	9.92	2.94	5.19	19.15	18.34	22.19	1.40	4.95	12.32	370.72	32.59
4938	113.30	1.40	37.95	11.04	4.49	6.72	24.98	10.00	21.15	1.10	5.32	27.14	*498.66*	32.86
4950	147.04	1.58	34.97	8.69	4.88	7.56	21.12	76.40	26.71	0.93	8.45	27.90	426.66	28.54
4962	41.18	4.51	183.04	110.39	2.78	8.32	123.96	35.80	42.10	2.49	*201.12*	125.00	203.47	26.74
4969	51.82	1.13	21.87	5.95	2.50	4.86	14.62	62.89	34.01	0.80	74.92	401.29	*637.42*	14.04
4997	120.94	1.36	34.47	14.58	3.07	7.50	17.54	26.56	33.25	1.18	5.75	59.42	335.26	34.14
41009	161.14	1.70	44.27	12.21	2.78	10.90	34.08	43.78	30.01	1.04	5.91	23.42	426.86	30.50
41010	***25.81***	***4.23***	***25.15***	***9.23***	***6.13***	***12.36***	***13.43***	***48.95***	***17.99***	***3.22***	***4.76***	***87.22***	***265.73***	***9.66***
KGS 998	116.84	1.64	37.76	10.46	6.33	9.34	19.96	55.28	29.67	1.08	5.60	13.35	287.41	28.29
hard coal	82	12	170	120	37	100	110	170	36	18	82	740	230	22
x2	*164*	*24*	*340*	*240*	*74*	*200*	*220*	*340*	*72*	*36*	*164*	*1480*	*460*	*44*
x5	***410***	***60***	***850***	***600***	***185***	***500***	***550***	***850***	***180***	***90***	***410***	***3700***	***1150***	***110***

KGS Kentucky Geological Survey

Tonsteins in regular type, floor rocks in blue italics, and coal in bold blue italics

without a distinct Ce anomaly). All of the latter samples comprise the highest normalized Lu values. Basically, all of the other samples have similar spider plots, varying in their normalized REE but not in the distribution patterns. Most of the samples have L-type distributions (the exceptions being 4703, 4823, 4962, and 41010) and negative Eu anomalies (the exceptions being 4703 and 4962; Figs. 10 and 11).

Table 5 Sample; ash basis (μg/g) minor elements from Mo through U; World coal average (ash basis), 2×World coal average, and 5×World coal average at bottom of table (after Ketris & Yudovich, 2009).

Sample	Mo	Ag	Cd	In	Sn	Sb	Cs	Ba	Hf	Ta	W	Tl	Pb	Bi	Th	U
	ash basis (μg/g)															
4647	1.39	*1.66*	0.62	0.19	13.8	0.43	2.20	110.3	12.8	*5.90*	3.79	0.20	42.2	0.32	24.6	7.2
4662	0.81	*2.11*	0.78	0.21	*16.9*	0.22	0.68	136.9	15.1	*4.05*	3.43	0.07	51.4	0.13	20.7	5.0
4673	5.27	*1.91*	0.70	0.15	12.2	0.06	1.66	338.9	13.1	3.07	1.20	0.44	63.2	dl	34.8	8.7
4687	0.24	*1.55*	0.62	0.13	12.6	0.06	0.36	123.5	14.2	3.77	2.16	0.05	50.5	dl	13.3	5.9
4703	*0.50*	*1.84*	*0.59*	*0.07*	*6.3*	*0.83*	*13.12*	*570.5*	*9.6*	*2.44*	*2.16*	*1.09*	*20.0*	*dl*	*11.9*	*3.7*
4712	0.18	*1.90*	0.75	0.21	13.1	0.12	0.37	214.6	16.1	3.52	1.90	0.17	52.9	0.18	26.1	5.3
4724	0.25	*1.89*	0.72	0.17	14.1	0.84	0.27	123.1	16.5	3.60	1.10	0.25	58.3	0.05	11.3	7.2
4734	0.25	*1.39*	0.61	0.12	11.8	0.36	0.39	210.2	10.5	3.62	2.93	0.08	50.8	dl	10.7	3.4
4746	0.24	*1.52*	0.71	0.18	11.6	dl	0.71	250.3	14.0	2.84	3.54	0.03	12.3	0.55	12.7	4.9
4761	1.18	*1.56*	0.71	0.18	12.8	0.11	0.48	154.9	15.6	3.88	1.64	0.12	46.4	dl	16.4	4.6
4777	0.63	1.23	0.56	0.12	11.9	0.28	0.21	66.9	12.1	*4.88*	2.74	0.21	50.5	dl	11.1	6.9
4790	0.30	*1.81*	0.64	0.10	11.0	0.12	0.39	113.9	14.6	3.84	3.68	0.09	51.6	dl	11.8	5.3
4806	1.24	*2.33*	0.80	0.15	13.6	0.40	0.77	115.5	16.6	*4.70*	4.22	0.10	38.1	0.00	21.1	4.2
4813	0.30	*1.77*	0.83	0.12	9.5	0.08	0.27	21.5	13.7	3.68	3.27	0.04	56.3	dl	9.2	6.0
4823	1.20	*1.64*	0.66	0.15	15.1	0.09	0.42	196.4	16.3	3.82	1.81	0.18	57.1	dl	12.8	7.1
4837	0.21	*1.55*	0.64	0.14	13.7	1.09	0.40	239.7	14.7	3.76	1.68	0.29	72.0	dl	23.0	7.9
4851	0.16	*1.41*	0.67	0.13	12.7	0.07	0.40	91.3	13.9	3.95	3.13	0.04	61.8	dl	19.3	4.6
4868	*dl*	*1.16*	*0.45*	*0.12*	*10.2*	*0.04*	*2.99*	*251.8*	*11.1*	*2.96*	*2.67*	*0.48*	*43.5*	*dl*	*25.3*	*5.1*
4879	0.30	*1.53*	0.55	0.21	11.6	0.17	1.14	107.8	13.9	3.65	2.68	0.15	58.5	0.13	11.0	3.2
4880	*0.09*	*0.62*	*0.33*	*0.15*	*6.4*	*0.29*	*14.39*	*874.5*	*6.3*	*1.58*	*2.25*	*1.32*	*26.0*	*0.33*	*26.4*	*6.5*
4887	2.30	*1.59*	0.66	0.12	12.8	0.07	0.37	71.3	12.8	3.73	2.66	0.23	48.4	dl	11.7	4.6
4895	0.76	*2.12*	0.73	0.11	13.8	0.59	0.35	52.2	15.4	*5.09*	3.71	0.10	46.1	dl	5.3	4.9
4911	0.41	*1.45*	0.56	0.17	10.2	0.41	4.70	218.1	8.9	2.84	2.69	1.10	43.4	0.01	28.1	6.6
4912	*0.10*	*1.13*	*0.45*	*0.11*	*10.7*	*0.19*	*2.39*	*166.6*	*11.2*	*3.27*	*3.02*	*0.49*	*52.9*	*dl*	*20.7*	*4.1*
4925	0.49	*1.63*	0.59	0.11	14.6	0.67	0.28	68.2	13.9	3.75	2.44	0.11	47.0	dl	5.8	5.8
4938	10.07	*2.20*	0.74	0.08	10.4	0.04	0.28	93.2	17.6	4.11	3.00	0.27	43.2	dl	11.0	7.6
4950	1.13	*1.80*	0.89	0.24	13.5	0.09	0.60	83.2	17.3	3.83	1.59	0.21	61.0	0.06	12.5	7.6
4962	1.04	0.88	0.34	0.13	11.0	1.13	17.28	700.2	6.4	2.44	2.69	1.22	26.0	0.44	19.4	4.8
4969	0.03	*1.46*	0.72	0.23	13.7	dl	2.71	647.2	15.0	2.64	0.22	0.37	54.2	0.80	*66.2*	14.8
4997	1.25	*1.46*	0.62	0.26	*42.3*	dl	0.56	203.2	12.8	3.60	2.73	0.08	63.3	dl	15.1	5.8
41009	0.37	*1.81*	0.79	0.21	16.1	0.02	0.41	85.1	17.1	3.91	1.89	0.11	44.9	dl	6.5	8.7
41010	*0.61*	*Dl*	*0.42*	*0.05*	*5.3*	*0.24*	*0.34*	*111.4*	*4.8*	*0.59*	*1.27*	*0.03*	*12.1*	*0.14*	*16.7*	*5.1*
KGS 998	2.82	1.10	0.57	1.32	389.7	0.20	0.44	93.7	13.6	3.82	1.57	0.24	51.63	dl	20.0	7.22
hard coal	14	0.63	1.2	0.21	8.0	7.5	8.0	900	9	2.00	7.8	4.6	55	7.5	23	15
x2	*28*	*1.26*	*2.4*	*0.42*	*16.0*	*15.0*	*16.0*	*1800*	*18*	*4*	*15.6*	*9.2*	*110*	*15.0*	*46.0*	*30.0*
x5	**70**	**3.15**	**6.0**	**1.05**	**40.0**	**37.5**	**40.0**	**4500**	**45**	**10**	**39**	**23.0**	**275**	**37.5**	**115.0**	**75.0**

KGS Kentucky Geological Survey

Tonsteins in regular type, floor rocks in blue italics, and coal in bold blue italics

While the Ce_N/Ce_N^* vs. Eu_N/Eu_N^* and Gd_N/Gd_N^* vs. Eu_N/Eu_N^* trends show flat, non-significant distributions for the tonstein samples, the Gd_N/Gd_N^* vs. Ce_N/Ce_N^* (Fig. 12) plot shows a positive correlation ($r^2 = 0.59$ with the inclusion of sample 4746 (a weathered tonstein; significant at the 1% level); $r^2 = 0.36$ (below the $r^2 = 0.37$ point for being significant at the 5% level). Removing the weathered and gradational tonsteins from consideration yields an $r^2 = 0.46$ which is significant at the 5% level. Sample

Table 6 Sample; ash basis (µg/g) REE plus Sc and Y; World coal average (ash basis), $2 \times$ World coal average, and $5 \times$ World coal average at bottom of table (after Ketris & Yudovich, 2009)

Ash basis (µg/g)																
Sample	Sc	Y	La	Ce	Pr	Nd	Sm	Eu	Gd	Tb	Dy	Ho	Er	Tm	Yb	Lu
4647	2.97	18.9	42.3	59.8	10.8	40.7	8.0	0.70	7.46	1.02	5.30	0.88	2.25	0.29	1.83	0.26
4662	1.43	12.5	25.6	26.2	6.8	26.2	5.3	0.40	4.74	0.66	3.48	0.57	1.50	0.17	1.21	0.16
4673	3.34	46.1	68.8	127.6	21.2	80.0	15.7	0.89	14.62	2.02	10.93	1.90	5.14	0.65	4.12	0.54
4687	1.61	15.9	24.1	24.0	6.9	26.8	5.3	0.33	4.83	0.68	3.85	0.67	1.83	0.23	1.49	0.19
4703	*15.89*	*41.2*	*48.4*	*100.7*	*11.3*	*43.1*	*8.0*	*1.64*	*8.50*	*1.19*	*7.27*	*1.46*	*4.41*	*0.62*	*4.44*	*0.66*
4712	2.79	30.5	46.5	44.1	13.7	53.5	11.0	0.75	10.19	1.41	7.47	1.26	3.32	0.40	2.58	0.34
4724	1.74	20.8	28.0	22.1	8.5	33.5	7.0	0.44	6.38	0.93	5.20	0.90	2.45	0.32	2.09	0.27
4734	1.06	5.7	13.9	17.5	3.7	14.0	2.6	0.22	2.31	0.28	1.49	0.23	0.63	0.07	0.52	0.07
4746	1.08	2.6	12.0	34.8	2.8	11.4	1.8	0.12	1.78	0.17	0.81	0.12	0.34	0.04	0.37	0.05
4761	1.63	20.2	35.8	39.8	10.1	39.6	7.8	0.42	7.24	1.00	5.33	0.90	2.38	0.29	1.92	0.25
4777	0.76	10.7	22.3	21.4	6.6	25.8	4.9	0.29	4.34	0.59	2.88	0.51	1.21	0.17	0.87	0.14
4790	0.96	6.8	14.0	18.9	3.9	15.3	2.8	0.18	2.61	0.33	1.77	0.30	0.77	0.09	0.56	0.07
4806	1.51	16.5	32.8	28.5	8.8	33.3	6.7	0.50	5.90	0.86	4.54	0.75	1.96	0.24	1.54	0.21
4813	0.55	3.7	15.2	19.3	4.0	15.4	2.7	0.14	2.28	0.25	1.15	0.16	0.41	0.03	0.27	0.03
4823	1.53	17.0	24.0	29.7	7.3	28.7	5.8	0.36	5.64	0.83	4.83	0.87	2.38	0.30	2.00	0.26
4837	2.05	22.8	33.8	36.3	9.4	36.4	7.1	0.47	6.54	0.93	5.38	0.97	2.68	0.34	2.24	0.28
4851	1.39	12.4	25.7	28.4	7.1	27.8	5.2	0.29	4.70	0.62	3.30	0.55	1.47	0.17	1.14	0.14
4868	*4.04*	*28.2*	*52.3*	*32.8*	*13.6*	*50.0*	*9.3*	*0.87*	*8.54*	*1.16*	*6.59*	*1.19*	*3.27*	*0.41*	*2.68*	*0.36*
4879	1.61	7.5	16.8	20.8	4.6	17.8	3.4	0.34	3.08	0.40	2.09	0.35	1.00	0.12	0.92	0.12
4880	*16.72*	*46.3*	*110.4*	*257.1*	*26.5*	*106.6*	*20.6*	*2.51*	*18.92*	*2.28*	*12.21*	*1.98*	*5.71*	*0.72*	*4.99*	*0.62*
4887	1.19	8.8	14.9	17.6	4.5	17.7	3.5	0.18	3.19	0.41	2.17	0.36	0.92	0.10	0.67	0.08
4895	0.75	4.0	9.6	12.2	2.5	9.5	1.7	0.09	1.54	0.18	1.00	0.15	0.41	0.04	0.33	0.04
4911	6.72	34.9	59.6	111.6	13.9	49.5	9.0	0.91	8.85	1.23	7.25	1.38	4.00	0.54	3.59	0.51
4912	*4.90*	*24.1*	*41.9*	*41.1*	*10.4*	*38.0*	*6.9*	*0.75*	*6.65*	*0.91*	*5.26*	*0.98*	*2.86*	*0.38*	*2.58*	*0.35*
4925	0.56	6.1	14.2	19.7	3.9	15.0	2.7	0.12	2.45	0.30	1.53	0.25	0.64	0.06	0.47	0.05
4938	0.99	5.0	16.9	35.8	4.6	17.5	3.1	0.15	2.81	0.31	1.47	0.22	0.54	0.05	0.37	0.04
4950	0.48	6.8	19.2	27.4	4.8	18.5	3.3	0.13	3.05	0.35	1.79	0.28	0.76	0.08	0.55	0.07
4962	19.58	35.7	63.1	125.3	13.9	51.4	8.9	1.74	8.60	1.08	6.30	1.27	4.07	0.58	4.30	0.66
4969	6.78	73.7	128.4	*286.0*	33.7	122.3	24.3	1.49	23.38	2.92	17.93	2.85	8.79	1.04	7.23	0.82
4997	1.30	12.7	20.0	29.3	5.4	20.9	4.0	0.25	3.83	0.52	3.03	0.54	1.49	0.19	1.24	0.15
41009	0.58	4.9	12.6	23.1	3.9	15.5	2.9	0.13	2.66	0.34	1.77	0.28	0.73	0.08	0.54	0.06
41010	***6.18***	***60.3***	***61.0***	***139.2***	***15.6***	***61.1***	***12.3***	***0.88***	***12.49***	***1.83***	***11.31***	***2.27***	***6.95***	***0.95***	***6.63***	***0.94***
KGS 998	1.38	28.7	56.9	41.0	15.3	59.3	11.6	0.68	10.6	1.44	7.49	1.23	3.07	0.36	2.17	0.27
hard coal	24	57	76	140	26	75	14	2.6	16	2.1	15	4.8	6.4	2.2	6.9	1.3
×2	*48*	*114*	*152*	*280*	*52*	*150*	*28*	*5.2*	*32*	*4.2*	*30.0*	*9.6*	*12.8*	*4.4*	*13.8*	*2.6*
×5	***120***	***285***	***380***	***700***	***130***	***375***	***70***	***13.0***	***80***	***10.5***	***75.0***	***24.0***	***32.0***	***11.0***	***34.5***	***6.5***

KGS Kentucky Geological Survey

Tonsteins in regular type, floor rocks in blue italics, and coal in bold blue italics

⧂ Springer

41010, the coal with tonstein-like inclusions, and the coal samples from the 4754–4765 series (data from Hower et al., 1999) exhibit a non-significant distribution to the low-Gd_N/Gd_N* side of the tonstein distribution indicating that the tonstein has a more pronounced M-type-distribution tendency than the coals.

Principal components analysis (PCA) (JMP® Pro 17.0.0, © JMP Statistical Discovery LLC, Cary, North Carolina, USA) for all of the samples shows that the first Eigenvector, contributing to 42.71% of the variation, comprises Al_2O_3/TiO_2, LREE/HREE, and Gd_N/Gd_N* with a less significant contribution by Zr+Nb (Fig. 13a; supporting statistics in Table 9). The second Eigenvector, contributing to 25.80% of the variation, is composed of Al_2O_3/TiO_2 and REE (ppm; ash basis) with a less significant contribution of Zr+Nb. The most significant outliers are 4703, 4746, 4806, 4969, and 4880, the weathered tonsteins and floor samples noted above (Fig. 13b). Without the floor and coal samples, the first Eigenvector, contributing to 42.96% of the variation, is comprised of Zr+Nb, LREE/HREE, and Gd_N/Gd_N*

Table 7 Sample; UCC-normalized REE values (after Taylor & McLennan, 1985)

	UCC-normalized REE													
Sample	La	Ce	Pr	Nd	Sm	Eu	Gd	Tb	Dy	Ho	Er	Tm	Yb	Lu
4647	1.41	0.93	1.53	1.57	1.79	0.80	1.96	1.70	1.51	1.10	0.98	0.97	0.83	0.86
4662	0.85	0.41	0.96	1.01	1.18	0.45	1.25	1.10	1.00	0.71	0.65	0.58	0.55	0.52
4673	2.29	1.99	2.98	3.08	3.49	1.01	3.85	3.36	3.12	2.38	2.24	2.17	1.87	1.79
4687	0.80	0.38	0.98	1.03	1.18	0.38	1.27	1.14	1.10	0.84	0.80	0.76	0.68	0.65
4703	*1.61*	*1.57*	*1.59*	*1.66*	*1.78*	*1.87*	*2.24*	*1.98*	*2.08*	*1.83*	*1.92*	*2.06*	*2.02*	*2.20*
4712	1.55	0.69	1.93	2.06	2.44	0.85	2.68	2.34	2.13	1.58	1.45	1.33	1.17	1.13
4724	0.93	0.34	1.20	1.29	1.55	0.50	1.68	1.55	1.49	1.13	1.06	1.05	0.95	0.91
4734	0.46	0.27	0.51	0.54	0.58	0.25	0.61	0.47	0.43	0.29	0.27	0.22	0.24	0.23
4746	0.40	0.54	0.40	0.44	0.41	0.14	0.47	0.28	0.23	0.15	0.15	0.14	0.17	0.15
4761	1.19	0.62	1.42	1.52	1.73	0.48	1.90	1.67	1.52	1.13	1.03	0.98	0.87	0.82
4777	0.74	0.33	0.93	0.99	1.08	0.33	1.14	0.99	0.82	0.63	0.53	0.57	0.39	0.47
4790	0.47	0.30	0.55	0.59	0.63	0.20	0.69	0.55	0.51	0.37	0.34	0.29	0.26	0.24
4806	1.09	0.45	1.24	1.28	1.48	0.56	1.55	1.43	1.30	0.94	0.85	0.78	0.70	0.69
4813	0.51	0.30	0.57	0.59	0.59	0.16	0.60	0.41	0.33	0.20	0.18	0.11	0.12	0.11
4823	0.80	0.46	1.03	1.11	1.29	0.41	1.48	1.38	1.38	1.08	1.03	1.02	0.91	0.87
4837	1.13	0.57	1.33	1.40	1.58	0.53	1.72	1.55	1.54	1.21	1.17	1.12	1.02	0.95
4851	0.86	0.44	1.01	1.07	1.16	0.33	1.24	1.03	0.94	0.69	0.64	0.57	0.52	0.48
4868	*1.74*	*0.51*	*1.91*	*1.92*	*2.07*	*0.99*	*2.25*	*1.94*	*1.88*	*1.49*	*1.42*	*1.36*	*1.22*	*1.19*
4879	0.56	0.32	0.65	0.68	0.75	0.38	0.81	0.66	0.60	0.43	0.44	0.41	0.42	0.41
4880	*3.68*	*4.02*	*3.73*	*4.10*	*4.57*	*2.85*	*4.98*	*3.80*	*3.49*	*2.48*	*2.48*	*2.39*	*2.27*	*2.08*
4887	0.50	0.27	0.64	0.68	0.77	0.21	0.84	0.69	0.62	0.45	0.40	0.33	0.30	0.27
4895	0.32	0.19	0.35	0.37	0.38	0.11	0.40	0.30	0.29	0.19	0.18	0.13	0.15	0.13
4911	1.99	1.74	1.96	1.91	2.00	1.03	2.33	2.05	2.07	1.72	1.74	1.81	1.63	1.70
4912	*1.40*	*0.64*	*1.47*	*1.46*	*1.54*	*0.85*	*1.75*	*1.51*	*1.50*	*1.23*	*1.24*	*1.26*	*1.17*	*1.16*
4925	0.47	0.31	0.54	0.58	0.60	0.14	0.65	0.50	0.44	0.31	0.28	0.21	0.21	0.18
4938	0.56	0.56	0.64	0.67	0.68	0.17	0.74	0.51	0.42	0.27	0.23	0.16	0.17	0.14
4950	0.64	0.43	0.68	0.71	0.73	0.15	0.80	0.58	0.51	0.35	0.33	0.26	0.25	0.23
4962	2.10	1.96	1.95	1.98	1.97	1.97	2.26	1.79	1.80	1.59	1.77	1.93	1.95	2.21
4969	4.28	4.47	4.75	4.70	5.39	1.69	6.15	4.86	5.12	3.56	3.82	3.46	3.28	2.72
4997	0.67	0.46	0.76	0.80	0.90	0.28	1.01	0.87	0.87	0.67	0.65	0.62	0.56	0.51
41009	0.42	0.36	0.55	0.60	0.64	0.14	0.70	0.56	0.51	0.36	0.32	0.25	0.25	0.21
41010	***2.03***	***2.17***	***2.19***	***2.35***	***2.74***	***1.00***	***3.29***	***3.05***	***3.23***	***2.84***	***3.02***	***3.18***	***3.02***	***3.12***
KGS 998	1.90	0.64	2.16	2.28	2.58	0.77	2.80	2.40	2.14	1.54	1.34	1.19	0.99	0.91

KGS Kentucky Geological Survey

Tonsteins in regular type, floor rocks in blue italics, and coal in bold blue italics

(Fig. 14a; supporting statistics in Table 10). The second Eigenvector, contributing to 34.02% of the variation, consists of Al_2O_3/TiO_2, Zr + Nb, and REE. The outliers are the weathered tonsteins (Fig. 14b).

In previous studies, the relationship between Al_2O_3/TiO_2 and REE (Dai et al., 2018) was used to discern a relationship, e.g. the REE distribution and the detrital minerals (represented, in part, by TiO_2). The Al_2O_3/TiO_2 vs. REE relationships is shown in Fig. 15 but it does not show a significant distribution among the tonstein samples. Samples 4703 and 4969, distinct outliers, are weathered tonsteins.

Other Elements

Zircons can contribute REE and Y to a coal as a detrital or tuffaceous mineral. Zircons were noted in the Fire Clay tonstein by Hower et al.

Table 8 Sample; Light (L) vs. Heavy (H) distribution, EuN/EuN*, CeN/CeN*, GdN/GdN*, total REE, REE + Y (REY), REY + Sc (REYSc, Light REE/Heavy REE (LREE/HREE)

Sample	Dist.	Eu_N/Eu_N*	Ce_N/Ce_N*	Gd_N/Gd_N*	REE	REY	REYSc	LREE/HREE
4647	L	0.46	0.64	1.14	182	201	203	8.09
4662	L	0.39	0.45	1.11	103	115	117	6.99
4673	L	0.29	0.76	1.13	354	400	404	7.68
4687	L	0.32	0.42	1.10	101	117	119	6.18
4703	*H*	*1.01*	*0.98*	*1.17*	*242*	*283*	*299*	*7.00*
4712	L	0.35	0.40	1.13	196	227	230	6.09
4724	L	0.32	0.32	1.08	118	139	141	5.22
4734	L	0.45	0.56	1.20	57	63	64	8.89
4746	L	0.38	1.36	1.46	67	69	70	16.54
4761	L	0.28	0.48	1.13	153	173	175	6.75
4777	L	0.32	0.40	1.12	92	103	103	7.36
4790	L	0.33	0.58	1.20	62	69	69	8.25
4806	L	0.39	0.38	1.07	126	143	145	6.68
4813	L	0.29	0.56	1.28	61	65	66	12.00
4823	H	0.31	0.51	1.10	113	130	132	5.47
4837	L	0.34	0.46	1.11	143	166	168	6.21
4851	L	0.30	0.48	1.16	107	119	120	7.60
4868	*L*	*0.49*	*0.28*	*1.14*	*183*	*211*	*215*	*6.30*
4879	L	0.53	0.54	1.17	72	79	81	7.52
4880	*L*	*0.66*	*1.08*	*1.23*	*571*	*617*	*634*	*10.44*
4887	L	0.28	0.48	1.18	66	75	76	7.21
4895	L	0.30	0.57	1.25	39	43	44	9.39
4911	L	0.51	0.88	1.15	272	307	313	8.62
4912	*L*	*0.55*	*0.45*	*1.15*	*159*	*183*	*188*	*6.68*
4925	L	0.24	0.61	1.22	61	67	68	9.42
4938	L	0.27	0.93	1.31	84	89	90	13.07
4950	L	0.21	0.65	1.27	80	87	88	10.39
4962	H	1.03	0.97	1.22	291	327	346	9.18
4969	L	0.32	0.99	1.22	661	735	742	8.95
4997	L	0.32	0.64	1.15	91	104	105	7.09
41009	L	0.23	0.74	1.19	65	70	70	8.81
41010	*H*	*0.35*	*1.03*	*1.11*	*333*	*394*	*400*	*6.53*
KGS 998	L	1.00	0.96	1.09	212	240	242	6.73

KGS Kentucky Geological Survey

Tonsteins in regular type, floor rocks in blue italics, and coal in bold blue italics
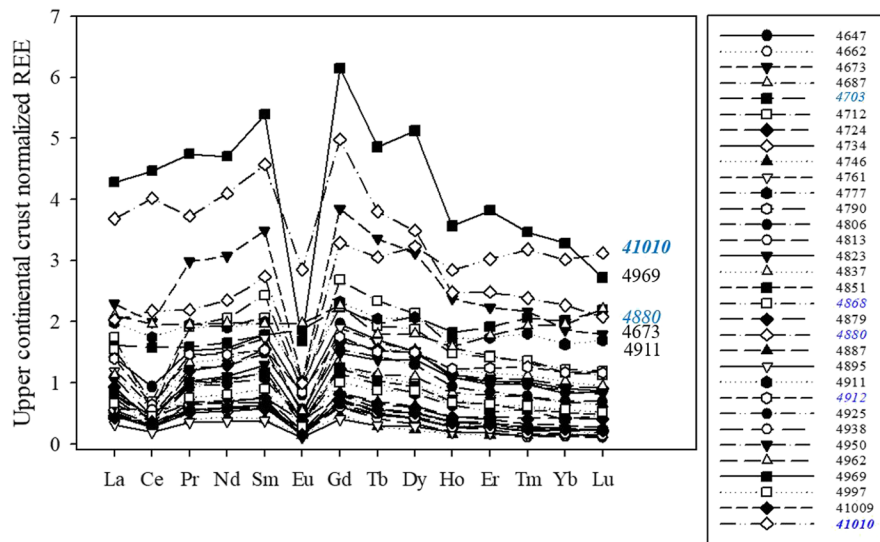
Fig. 10 Upper continental crust-normalized REE distributions for all of the studied samples. Normalization after Taylor & McLennan (1985)

(1994) and in the present study. The relationship between Zr + Nb (ppm; ash basis) and Al_2O_3/TiO_2 (after Dai et al., 2018), with the TiO_2 being an indicator of detrital contributions and a trace mineral in tuffaceous deposition (Hower et al., 1994), is shown in Fig. 16. Within the tonstein population, excluding the weathered samples (4703, 4962, and 4969), there is a clustering of the points but there is no significant relationship, with the Zr + Nb showing a greater relative variation than the Al_2O_3/TiO_2. Zircons can contain trace amounts of Y but the relationship between Zr and Y (Fig. 17) is not significant for these samples.
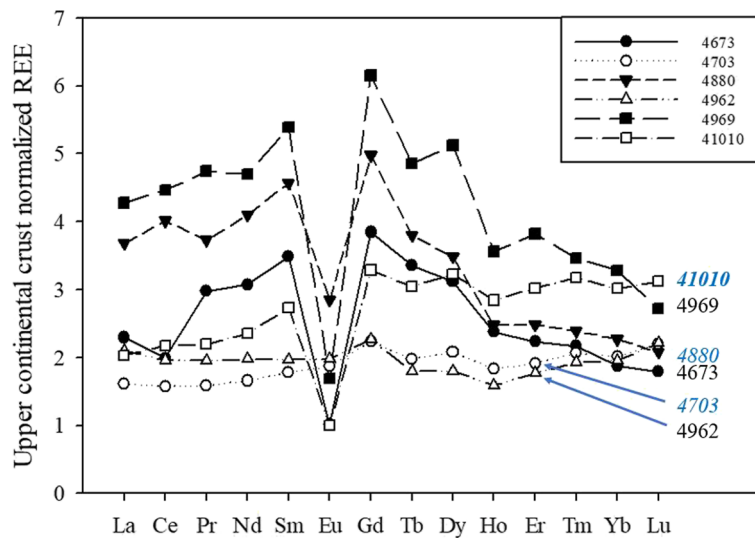
Fig. 11 Upper continental crust-normalized REE distributions for the samples with the highest normalized Lu. Normalization after Taylor & McLennan (1985)
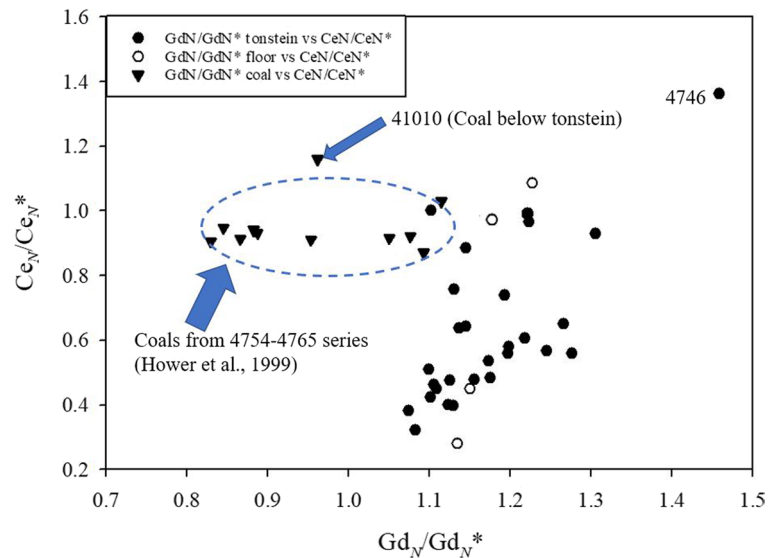
Fig. 12 Gd_N/Gd_N^* vs. Ce_N/Ce_N^* distribution showing the locations of coal data from Hower et al. (1999)

Compared with the world hard coal average (after Ketris & Yudovich, 2009) (admittedly, not necessarily the best baseline for the tonstein and floor samples, but they are within or adjacent to coal), few elements exceed even the $2\times$-world coal average level. Lithium reaches its highest concentrations at several Hazard South and Vicco quadrangle locations. Aside from Ag, with only one tonstein sample (weathered sample 4962) not reaching the $2\times$ level, only Zr and Ta exceed the $2\times$ level in five of the 27 tonstein samples. The greatest Ta concentrations correspond with some of the highest Nb samples (Fig. 18), with samples 4647, 4806, and 4895 all being from Vicco quadrangle sites. The largest Zr value corresponds with the largest Y value (weathered sample 4969; Fig. 17). The same sample also has the highest REE concentrations (except for Eu) and the largest Th and U contents of any of the tonstein samples. The high Zr, Y, REE, and Th + U in sample 4969 and, to a lesser extent, in sample 4962, might be a function of an enhanced concentration of zircons and REE-bearing minerals, such as monazite, in the weathered tonstein.

Discussion

The tonstein rock type, after Winchester and Floyd (1977) and later utilization of the defining geochemical parameters, is largely trachyandesite to trachyte (Fig. 19) and has a relatively constant Zr/TiO_2 value but Nb/Y values which change significantly, especially as there is little change in the designated fields, suggesting that tonsteins present in this study have all come from a very similar source.

The tonstein mineralogy is generally dominated by kaolinite (59–91% of the unweathered samples) with illite > quartz comprising the remainder of the major minerals. Much of the kaolinite is a secondary mineral after volcanic glass, as evidenced not only by its vermicular texture derived from other original volcanic minerals (e.g. mica; Dai et al., 2017c) but also by its matrix occurrence for other minerals rather than detrital modes of occurrence (Fig. 5) and in Hower et al. (2018), although phenocrysts of kaolinite suggest a primary deposition of those forms. Minor amounts of clinoptilolite, siderite, pyrite, gypsum, chlorite, and anatase were detected and quantified by XRD + Siroquant. Sanidine, apatite, zircon, ilmenite, pyrite, crandallite, florencite, galena, siderite, and goethite were detected by SEM among these samples. Monazite and kaolinite phenocrysts were noted in the electron microscopy study of the correlative Dean coal (Hower et al., 2018); Hower et al. (1994) found sanidine (some with alteration to quartz and kaolinite), β-quartz, magnetite, magnetite with an ilmenite core, anatase, rutile, and weathered titanite; and Robl and Bland (1977) noted

Springer

the presence of kaolinite pseudomorphs after β-quartz and sanidine. Mineralogical evidence for a volcanic-ash deposit includes vermicular kaolinite, sanidine, β-quartz, euhedral zircons, ilmenite, apatite, and phosphates including crandallite-group minerals, monazite. and rutile (or anatase). The possibility that some of the phosphates and TiO_2 minerals could be of secondary origin cannot be discounted. The Fe-Ti oxides shown in Fig. 7c,d give strong evidence for the magmatic origin of at least some of the Fe-Ti oxide/TiO_2 suite.

The tonstein geochemistry is dominated by Al_2O_3 and SiO_2, a function of the dominance of kaolinite. The total REE content, exceeding 400 µg/g in one case (sample 4997) and < 100 µg/g at many of the sites, is, perhaps, deceptively small as the REE in the coal is often reported on an ash basis (e.g. Hower

et al., 2016, 2020). The tonstein, with REE and REY-bearing minerals such as apatite, crandallite, monazite, florencite, and zircon, was, indeed, a primary source of the REE in the surrounding coal. That influence may have been through direct deposition of REY-bearing minerals, as in coal sample 41,010, or via remobilization of the REY in the tonstein by leaching.

Among the tonsteins, some of the highest REY concentrations occur in tonsteins that were possibly gradational with non-tonstein lithologies (samples 4673 and 4911; noted in both the megascopic appearance and in the < 40% kaolinite content) and in weathered outcrops (samples 4962 and 4969). The reasons for this could not be explored further in this study because crushed whole-rock samples were being
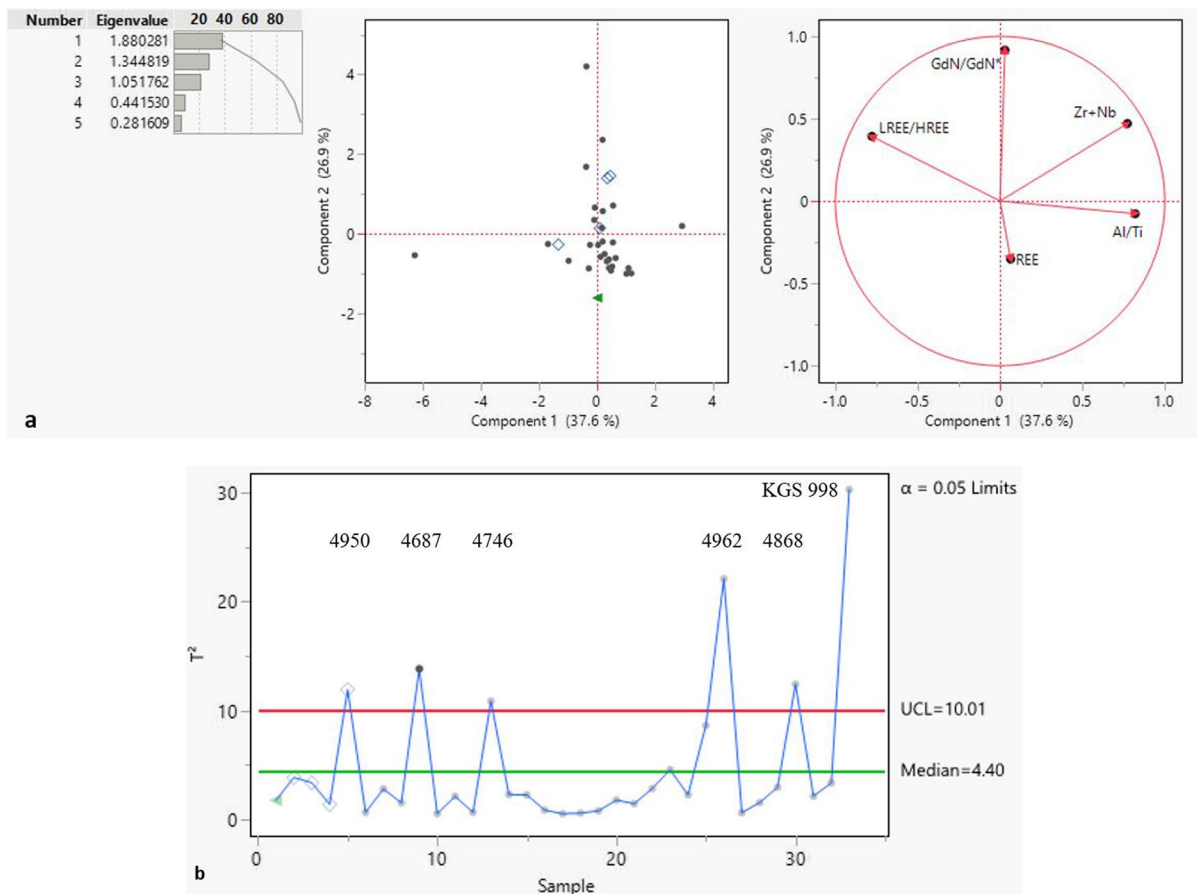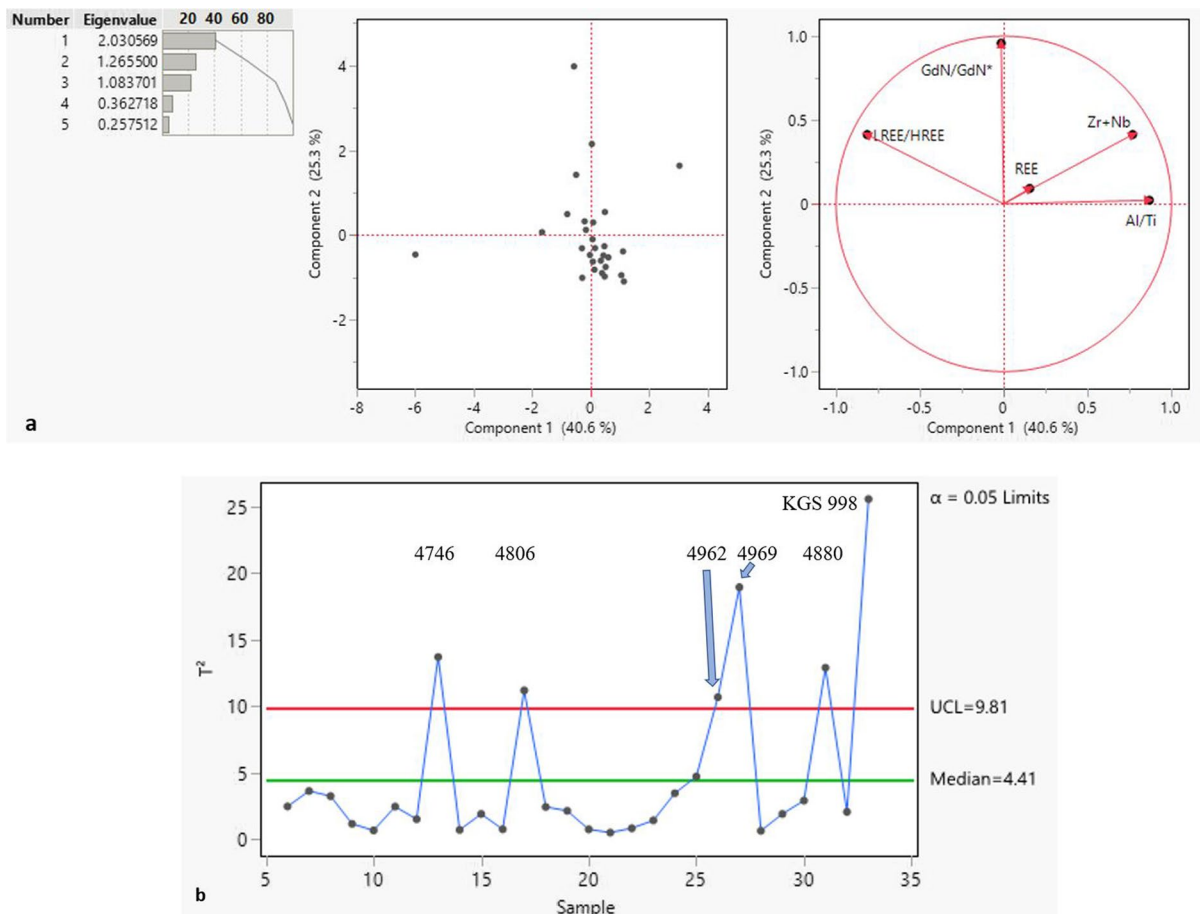

Fig. 13 a Principal components analysis (PCA) distribution for selected variables for all of the samples. Note that the vectors for LREE/HREE and Gd_N/Gd_N* overlap at this scale. **b** Outlier distribution for all samples

Table 9 Principal components analysis parameters for the analysis of all samples

Correlations

	Al/Ti	Zr + Nb	REE	LREE/HREE	Gd_N/Gd_{N*}
Al/Ti	1.0000	0.2029	0.2586	–0.1105	–0.0863
Zr + Nb	0.2029	1.0000	–0.0873	0.3147	0.2968
REE	0.2586	–0.0873	1.0000	–0.0358	–0.0662
LREE/HREE	–0.1105	0.3147	–0.0358	1.0000	0.9539
Gd_N/Gd_{N*}	–0.0863	0.2968	–0.0662	0.9539	1.0000

Covariance matrix

	Al/Ti	Zr + Nb	REE	LREE/HREE	Gd_N/Gd_{N*}
Al/Ti	23.169	87.503	180.283	–1.252	–0.033
Zr + Nb	87.503	8026.766	–1133.302	66.387	2.100
REE	180.283	–1133.302	20981.725	–12.201	–0.757
LREE/HREE	–1.252	66.387	–12.201	5.544	0.177
Gd_N/Gd_{N*}	–0.033	2.100	–0.757	0.177	0.006

Eigenvalues

Number	Eigenvalue	%	Cumul. %	Chi Square	d.f	Prob > ChiSq
1	2.136	42.706	42.706	79.829	9.344	< 0.0001
2	1.290	25.797	68.503	61.397	7.859	< 0.0001
3	0.965	19.301	87.804	50.302	4.937	< 0.0001
4	0.565	11.307	99.111	35.972	2.235	< 0.0001
5	0.044	0.889	100.000	0.000		

Eigenvectors

	Prin1	Prin2	Prin3	Prin4	Prin5
Al/Ti	–0.0750	0.7489	–0.2241	–0.6182	–0.0337
Zr + Nb	0.3483	0.3447	–0.6298	0.6022	0.0267
REE	–0.1028	0.5659	0.6832	0.4486	0.0335
LREE/HREE	0.6579	–0.0022	0.2158	–0.1220	–0.7112
Gd_N/Gd_{N*}	0.6555	–0.0073	0.1995	–0.1979	0.7009

Loading matrix

	Prin1	Prin2	Prin3	Prin4	Prin5
Al/Ti	–0.1096	0.8505	–0.2201	–0.4648	–0.0071
Zr + Nb	0.5089	0.3915	–0.6187	0.4528	0.0056
REE	–0.1503	0.6427	0.6712	0.3373	0.0071
LREE/HREE	0.9613	–0.0025	0.2120	–0.0917	–0.1499
Gd_N/Gd_{N*}	0.9579	–0.0073	0.1960	–0.1488	0.1478

analyzed. The character of these samples is seen in the upppermost UCC spidergram plots (Figs. 10 and 11), with the gradational and weathered tonsteins, the floor rock, and the coal sample having the greatest and, in some cases, the most significant, negative Eu anomalies. In the PCA analyses (Figs. 13b and 14b),

the weathered tonsteins are among the outliers. In the assessment of REE vs. Zr + Nb (Fig. 15), Al_2O_3/TiO_2 vs. Zr + Nb (Fig. 16), and Zr vs. Y (Fig. 17), weathered sample 4969 stands out as being distinctly different from the other tonstein samples. Both weathered samples are on the low-Ta and, to a lesser extent, the

low-Nb end of the Nb vs. Ta plot (Fig. 18). Transitional sample 4673 is at the low-Nb/Y and high-Zr-TiO$_2$ end of the Winchester and Floyd (1977) rock classification (Fig. 19).

What are the implications of the outliers? For the transitional tonsteins, the rock type was gradational between the tonstein, as represented by the apparently non-gradational samples with 59–92% kaolinite, and a relatively illite-rich lithology. In the deposition of the partings, the passage from an illitic clay to the kaolinite-rich tonstein can be seen (Fig. 2a,b); the boundary between the two is transitional, as seen by

the dark streaks in the lower quarter of the tonstein (Fig. 2b). The illitic clay, presumed to have been a terrigenous depositional event, is an influence on the REE chemistry of the coal underlying the tonstein, with the coal below the illitic clay having a lower REE content than coal directly underlying the ash-fall tonstein (Fig. 2c) (Hower et al., 1999, 2020). Weathering of the tonstein preferentially removes kaolinite from the rock, leaving behind REE-bearing phosphates (apatite, crandallite, florencite, monazite) and Y-bearing zircon, the latter causing a relative enrichment in the REY.

Fig. 14 **a** Principal components analysis (PCA) distribution for selected variables for the tonstein samples. Note that the vectors for LREE/HREE and Gd$_N$/Gd$_N$* overlap at this scale. **b** Outlier distribution for all samples

Table 10 Principal components analysis parameters for analysis of the tonstein

Correlations					
	Al/Ti	Zr + Nb	REE	LREE/HREE	Gd_N/Gd_{N*}
Al/Ti	1.0000	0.2826	0.5095	–0.1248	–0.0660
Zr + Nb	0.2826	1.0000	0.2394	0.3323	0.3160
REE	0.5095	0.2394	1.0000	–0.0957	–0.1096
LREE/HREE	–0.1248	0.3323	–0.0957	1.0000	0.9595
Gd_N/Gd_{N*}	–0.0660	0.3160	–0.1096	0.9595	1.0000
Covariance matrix					
	Al/Ti	Zr + Nb	REE	LREE/HREE	Gd_N/Gd_{N*}
Al/Ti	18.586	101.293	284.435	–1.320	–0.024
Zr + Nb	101.293	6913.085	2577.175	67.684	20.288
REE	284.435	2577.175	16770.319	–30.348	–1.193
LREE/HREE	–1.320	67.684	–30.348	6.001	0.198
Gd_N/Gd_{N*}	–0.024	20.288	–1.193	0.198	0.007

Eigenvalues						
Number	Eigenvalue	%	Cumul. %	Chi Square	d.f	Prob > ChiSq
1	2.148	42.955	42.955	78.244	9.103	< 0.0001
2	1.701	34.016	76.971	62.093	7.604	< 0.0001
3	0.625	12.503	89.474	37.445	5.214	< 0.0001
4	0.490	9.793	99.267	30.362	2.540	< 0.0001
5	0.037	0.734	100.001	0.000		

Eigenvectors					
	Prin1	Prin2	Prin3	Prin4	Prin5
Al/Ti	–0.0569	0.6444	0.1824	0.7367	0.0741
Zr + Nb	0.3443	0.4286	–0.8228	–0.1418	–0.0275
REE	–0.0716	0.6293	0.4119	–0.6538	–0.0413
LREE/HREE	0.6626	–0.0564	0.2289	–0.0275	0.7104
Gd_N/Gd_{N*}	0.6288	–0.0431	0.2603	0.0944	–0.6982
Loading matrix					
	Prin1	Prin2	Prin3	Prin4	Prin5
Al/Ti	–0.0834	0.8404	0.1442	0.5155	0.0142
Zr + Nb	0.5046	0.5589	–0.6505	–0.0992	–0.0053
REE	–0.1050	0.8207	0.3256	0.4575	–0.0076
LREE/HREE	0.9711	–0.0736	0.1810	–0.0193	0.1361
Gd_N/Gd_{N*}	0.9355	–0.0562	0.2058	0.0660	–0.1337

Summary

A lanthanide-rich, 315–317 Ma (after Machlus et al., 2020) volcanic ash-fall tonstein occurs in association with the Middle Pennsylvanian Duckmantian-age Fire Clay coal in eastern Kentucky. Ranging from 1.5 to nearly 29 cm in thickness in the study area, the tonstein was deposited generally during peat accumulation, although sites with the tonstein at the base of the coal or within the underclay are known. Outside of the study area, the ash fall is known to have been dispersed within the peat, resulting in REE-rich coal
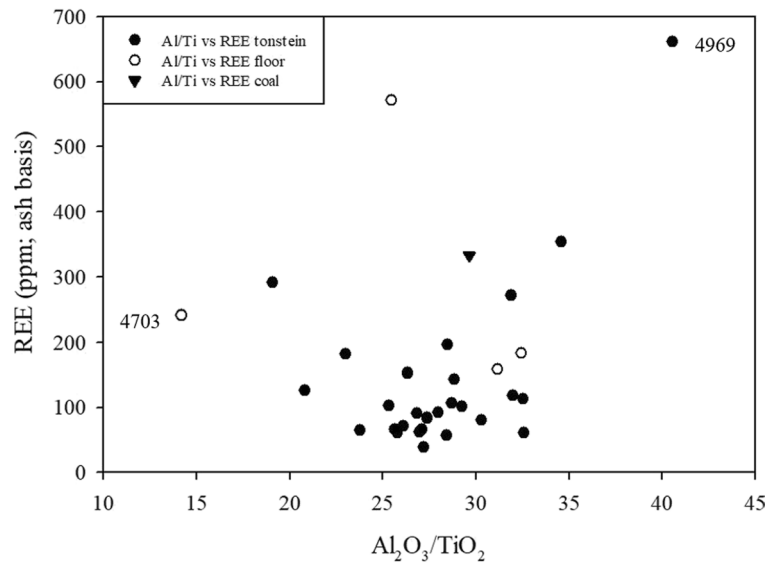
Fig. 15 REE vs. Zr + Nb (ppm; ash basis) for all samples
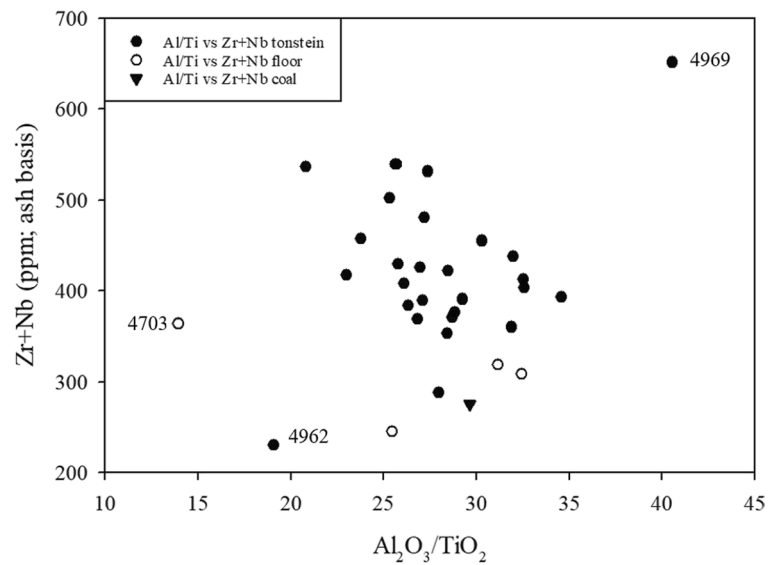
Fig. 16 Al$_2$O$_3$/TiO$_2$ vs. Zr + Nb (ppm; ash basis) for all samples
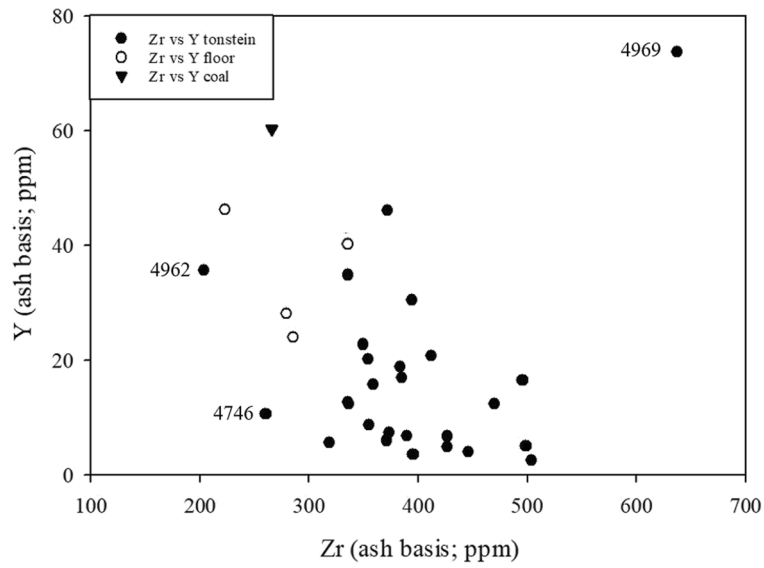
🖄 Springer

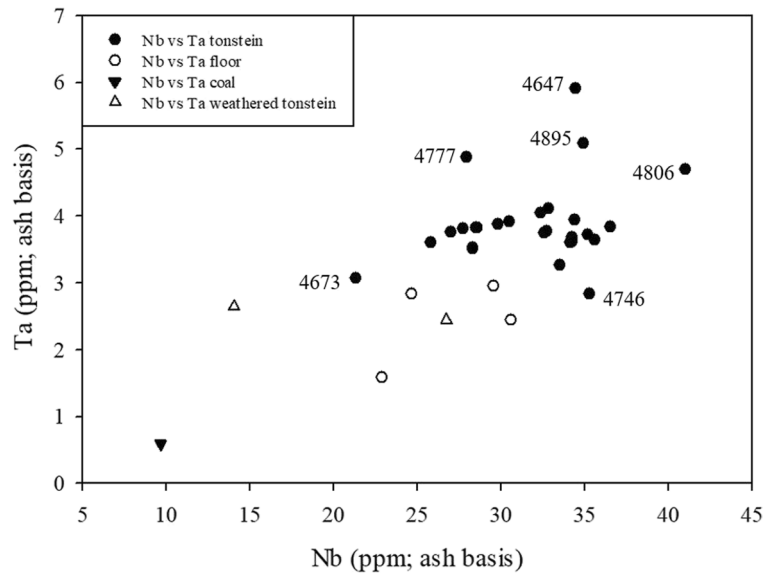**Fig. 17** Zr vs. Y (both ppm; ash basis) for all samples

Fig. 18 Nb vs. Ta (both ppm; ash basis) for tonstein, weathered tonstein, floor, and coal
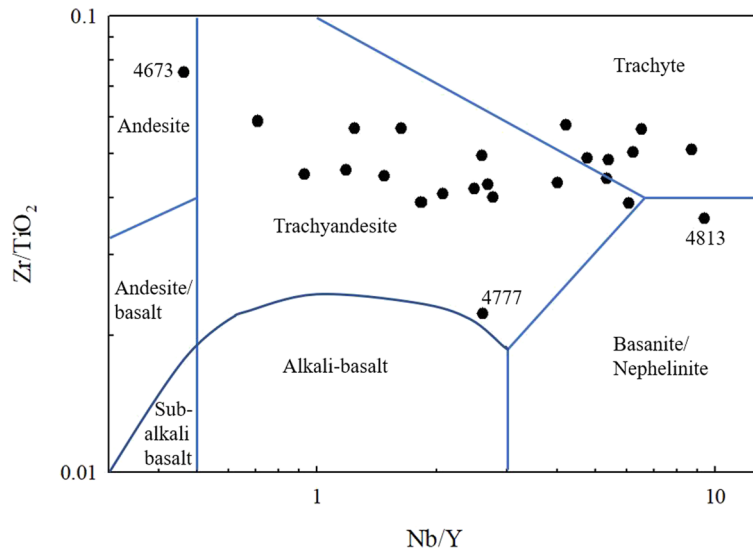
🖄 Springer

Fig. 19 Rock classification based on Nb/Y vs. Zr/TiO$_2$ after Winchester and Floyd (1977) and Vergunov et al. (2022)

lithologies but not as a distinct parting (Hower et al., 2018; Mardon & Hower, 2004). In addition to the tonstein, one coal and four floor (underclay) samples were studied.

Some of the tonsteins were transitional to illitic partings and two of the samples were from roadcuts (therefore, weathered samples). The kaolinite content of the non-weathered tonsteins and exclusive of the partings known to be transitional to other lithologies ranged from 50–92%. Illite and quartz were present as major to minor minerals in all cases, with clinoptilolite, siderite, pyrite, gypsum, chlorite, and anatase detected by XRD and Siroquant mineralogy; sanidine, apatite, zircon, ilmenite, pyrite, crandallite, florencite, galena, siderite, and goethite observed during SEM examination of three of the samples; and monazite, β-quartz, magnetite, magnetite with an ilmenite core, rutile, and weathered titanite known from studies by Robl and Bland (1977), Bohor and Triplehorn (1981, 1993), and Hower et al., (1994, 2018). Evidence for a volcanic-ash deposit includes vermicular kaolinite, sanidine, β-quartz, euhedral zircons, ilmenite, apatite, phosphates (including crandallite-group minerals and monazite), and rutile (or anatase). Zircons and the REE-bearing phosphates

contributed to the REY concentrations in the tonstein. The REE concentration is enriched in the weathered tonsteins due to the preservation of REE-bearing phosphates (apatite, crandallite, florencite, monazite) and Y-bearing zircon at the expense of the kaolinite weathered from the rock.

Authors' Contributions Liu, Dai, Dong, Gao – chemical, mineralogical, and SEM analyses; Berti – TEM analysis; Eble and Hower – collection of samples; Liu, Dai, Berti, Eble, Hower – writing of manuscript.

Data availability All of the data are available in the tables. The remaining samples are stored at the Kentucky Geological Survey's Earth Analysis Research Laboratory in Lexington, Kentucky, USA and at the China University of Mining & Technology.

Declarations

Conflicts of interest/Competing interests   The authors declare no conflict of interest or competing interests.

References

Aide, M. T., & Aide, C. (2012). Rare earth elements: Their importance in understanding soil genesis. *ISRN Soil Science, 2012*, article 783876. https://doi.org/10.5402/2012/783876

Andrews, W. M., Jr., Hower, J. C., & Hiett, J. K. (1994). Investigations of the Fire Clay coal bed, southeastern Kentucky, in the vicinity of sandstone washouts. *International Journal of Coal Geology, 26*, 95–115.

Arbuzov, S. I., Chekryzhov, I. Y., Verkhoturov, A. A., Spears, D. A., Melkiy, V. A., Zarubina, N. V., & Blokhin, M. G. (2023). Geochemistry and rare-metal potential of coals of the Sakhalin coal basin, Sakhalin island, Russia. *International Journal of Coal Geology, 268*, 104197.

ASTM Standard D3173/D3173M-17a. (2017). Test Method for Moisture in the Analysis Sample of Coal and Coke. ASTM International, West Conshohocken, PA, USA.

ASTM Standard D3174–12. (2018a). Annual Book of ASTM Standards. Test Method for Ash in the Analysis Sample of Coal and Coke. ASTM International, West Conshohocken, PA, USA.

ASTM Standard D4239–18e1. (2018b). Standard Test Method for Sulfur in the Analysis Sample of Coal and Coke Using High-Temperature Tube Furnace Combustion. ASTM International, West Conshohocken, PA, USA.

Bau, M., & Dulski, P. (1996). Distribution of yttrium and rare-earth elements in the Penge and Kuruman Iron-Formations, Transvaal Supergroup, South Africa. *Precambrian Research, 79*, 37–55.

Bish, D. L., & Von Dreele, R. B. (1989). Rietveld refinement of non-hydrogen atomic positions in kaolinite. *Clays and Clay Minerals, 37*, 289–296.

Bohor, B. F., & Triplehorn, D. M. (1981). Volcanic origin of the flint clay parting in the Hazard No. 4 (Fire Clay) coal bed of the Breathitt Formation in eastern Kentucky. In J.C.Cobb, et al., eds., *Coal and coal-bearing rocks of eastern Kentucky. Geological Society of America Coal Geology Division Field Trip*. Kentucky Geological Survey, Series XI, 49.

Bohor, B. F., & Triplehorn, D. M. (1993). Tonsteins: altered volcanic-ash layers in coal-bearing sequences. *Geological Society of America Special Paper*, 285, 44 pp.

Brownfield, M. E., Affolter, R. H., Cathcart, J. D., Johnson, S. Y., Brownfield, I. K., & Rice, C. A. (2005). Geologic setting and characterization of coals and the modes of occurrence of selected elements from the Franklin coal zone, Puget Group, John Henry No. 1 mine, King County, Washington, USA. *International Journal of Coal Geology, 63*, 247–275.

Chesnut, D. R. (1985). Source of the volcanic ash deposit (flint clay) in the Fire Clay coal of the Appalachian Basin. Dixiéme Congrés International de Stratigraphie et de Géologie du Carbonifére, Madrid, 1983, Compte Rendu 1, 145-154.

Dai, S., Ren, D., Chou, C.-L., Li, S., & Jiang, Y. (2006). Mineralogy and geochemistry of the No. 6 coal (Pennsylvanian) in the Junger Coalfield, Ordos Basin, China. *International Journal of Coal Geology, 66*, 253–270.

Dai, S., Li, D., Chou, C.-L., Zhao, L., Zhang, Y., Ren, D., Ma, Y., & Sun, Y. (2008). Mineralogy and geochemistry of boehmite-rich coals: New insights from the Haerwusu Surface Mine, Jungar Coalfield, Inner Mongolia, China. *International Journal of Coal Geology, 74*, 185–202.

Dai, S., Wang, X., Zhou, Y., Hower, J. C., Li, D., Chen, W., Zhu, X., & Zou, J. (2011). Chemical and mineralogical compositions of silicic, mafic, and alkali tonsteins in the late Permian coals from the Songzao Coalfield, Chongqing, Southwest China. *Chemical Geology, 282*, 29–44.

Dai, S., Zhang, W., Seredin, V. V., Ward, C. R., Hower, J. C., Wang, X., Li, X., Song, W., Zhao, L., Kang, H., Zheng, L., & Zhou, D. (2013a). Factors controlling geochemical and mineralogical compositions of coals preserved within marine carbonate successions: A case study from the Heshan Coalfield, southern China. *International Journal of Coal Geology, 109–110*, 77–100.

Dai, S., Zhang, W., Ward, C. R., Seredin, V. V., Hower, J. C., Li, X., Song, W., Wang, X., Kang, H., Zheng, L., Wang, P., & Zhou, D. (2013b). Mineralogical and geochemical anomalies of late Permian coals from the Fusui Coalfield, Guangxi Province, southern China: Influences of terrigenous materials and hydrothermal fluids. *International Journal of Coal Geology, 105*, 60–84.

Dai, S., Chekryzhov, I. Y., Seredin, V. V., Nechaev, V. P., Graham, I. T., Hower, J. C., Ward, C. R., Ren, D., & Wang, X. (2016a). Metalliferous coal deposits in East Asia (Primorye of Russia and South China): A review of geodynamic controls and styles of mineralization. *Gondwana Research, 29*, 60–82.

Dai, S., Graham, I. T., & Ward, C. R. (2016b). A review of anomalous rare earth elements and yttrium in coal. *International Journal of Coal Geology, 159*, 82–95.

Dai, S., Xie, P., Jia, S., Ward, C. R., Hower, J. C., Yan, X., & French, D. (2017a). Enrichment of U-Re-V-Cr-Se and rare earth elements in the Late Permian coals of the Moxinpo Coalfield, Chongqing, China: Genetic implications from geochemical and mineralogical data. *Ore Geology Reviews, 80*, 1–17.

Dai, S., Xie, P., Ward, C. R., Yan, X., Guo, W., French, D., & Graham, I. T. (2017b). Anomalies of rare metals in Lopingian super-high-organic-sulfur coals from the Yishan coalfield, Guangxi, China. *Ore Geology Reviews, 88*, 235–250.

Dai, S., Ward, C. R., Graham, I. T., French, D., Hower, J. C., Zhao, L., & Wang, X. (2017c). Altered volcanic ashes in coal and coal-bearing sequences: A review of their nature and significance. *Earth-Science Reviews, 175*, 44–74.

Dai, S., Nechaev, V. P., Chekryzhov, IYu., Zhao, L., Vysotskiy, S. V., Graham, I., Ward, C., Ignatiev, A. V., Velivetskaya, T. A., Zhao, L., French, D., & Hower, J. C. (2018). A model for Nb–Zr–REE–Ga enrichment in Lopingian altered alkaline volcanic ashes: Key evidence of H-O isotopes. *Lithos, 302–303*, 359–369.

Davis, B. A., Rodrigues, S., Esterle, J. S., Nguyen, A. D., Duxbury, A. J., & Golding, S. D. (2021). Geochemistry of apatite in Late Permian coals, Bowen Basin, Australia. *International Journal of Coal Geology, 237*, 103708.

Davranche, M., Grybos, M., Gruau, G., Pédrot, M., Dia, A., & Marsac, R. (2011). Rare earth element patterns: A tool for identifying trace metal sources during wetland soil reduction. *Chemical Geology, 284*, 127–137.

Dopita, M., & Kralik, J. (1977). Coal Tonsteins in Ostrava-Karvina Coal Basin (Uhelne Tonsteiny

🔆 Springer

Ostravsko-Karvinskeho Reviru). Ostrava, Czechoslova-
kia, 213 p.

Eble, C. F., Hower, J. C., & Andrews, W. M., Jr. (1994).
Paleoecology of the Fire Clay coal bed in a portion of
the Eastern Kentucky coal field. *Palaeogeography, Pal-
aeoclimatology, Palaeoecology, 106*, 287–305.

Eskenazy, G. (1978). Rare-earth elements in some coal basins
of Bulgaria. *Geologica Balcanica, 8*, 81–88.

Eskenazy, G. M. (1987a). Rare earth elements and yttrium in litho-
types of Bulgarian coals. *Organic Geochemistry, 11*, 83–89.

Eskenazy, G. M. (1987b). Zirconium and hafnium in Bulgarian
coals. *Fuel, 66*, 1652–1657.

Eskenazy, G. M. (1987c). Rare earth elements in a sampled
coal from the Pirin Deposit, Bulgaria. *International Jour-
nal of Coal Geology, 7*, 301–314.

Eskenazy, G. (1995). Geochemistry of rare earth elements in
Bulgarian coals. *Annuaire de l'Universite´ de Sofia '"St.
Kliment Ohridski"', Faculte´ de Geologie et Geographie.
Livre 1-Geologie, 88*, 39–65.

Eskenazy, G. M. (1999). Aspects of the geochemistry of rare
earth elements in coal: An experimental approach. *Inter-
national Journal of Coal Geology, 38*, 285–295.

Eskenazy, G. M. (2015). Sorption of trace elements on xylain:
An experimental study. *International Journal of Coal
Geology, 150–151*, 166–169.

Eskenazy, G. M., Mincheva, E. I., & Rousseva, D. P. (1986).
Trace elements in lignite lithotypes from the Elhovo coal
basin. *Comptes Rendus Del'académie Bulgare Des Sci-
ences, 39*(10), 99–101.

Given, P. H. (1984). An essay on the organic geochemistry of
coal. Academic Press. In *Coal Science* 3, (63–251, 339–
341). Academic Press, New York.

Greb, S. F., Eble, C. F., & Hower, J. C. (1999). Depositional
history of the Fire Clay coal bed (Late Duckmantian),
eastern Kentucky, USA. *International Journal of Coal
Geology, 40*, 255–280.

Greb, S. F., Eble, C. F., Hower, J. C., & Andrews, W. M.
(2002). Multiple-bench architecture and interpretations of
original mire phases in Middle Pennsylvanian coal seams:
Examples from the Eastern Kentucky coal field. *Interna-
tional Journal of Coal Geology, 49*, 147–175.

Guerra-Sommer, M., Cazzulo-Klepzig, M., Santos, J. O. S.,
Hartmann, L. A., Ketzer, J. M., & Formoso, M. L. L.
(2008). Radiometric age determination of tonsteins and
stratigraphic constraints for the Lower Permian coal suc-
cession in southern Paraná Basin, Brazil. *International
Journal of Coal Geology, 74*, 13–27.

Hatcher, P. G., & Clifford, D. J. (1996). The organic geochem-
istry of coal: From plant materials to coal. *Organic Geo-
chemistry, 27*, 251–274.

Hou, Y., Dai, S., Nechaev, V. P., Finkelman, R. B., Wang, H.,
Zhang, S., & Di, S. (2023). Mineral matter in the Penn-
sylvanian coal from the Yangquan Mining District, north-
eastern Qinshui Basin, China: Enrichment of critical ele-
ments and a Se-Mo-Pb-Hg assemblage. *International
Journal of Coal Geology, 266*, 104178.

Hower, J. C., Andrews, W. M., Jr., Wild, G. D., Eble, C. F.,
Dulong, F. T., & Salter, T. L. (1994). Coal quality trends
for the Fire Clay coal bed, southeastern Kentucky. *Journal
of Coal Quality, 13*, 13–26.

Hower, J. C., Berti, D., Hochella, M. F., Jr., & Mardon, S. M.
(2018). Rare Earth minerals in a "no tonstein" section of
the Dean (Fire Clay) coal, Knox County, Kentucky. *Inter-
national Journal of Coal Geology, 193*, 73–86. https://doi.
org/10.1016/j.coal.2018.05.001

Hower, J. C., & Bland, A. E. (1989). Geochemistry of the Pond
Creek Coal Bed, Eastern Kentucky Coalfield. *Interna-
tional Journal of Coal Geology, 11*, 205–226.

Hower, J. C., Eble, C. F., Backus, J. S., Xie, P., Liu, J., Fu, B., &
Hood, M. M. (2020). Aspects of rare earth element enrich-
ment in central appalachian coals. *Applied Geochemistry, 120*,
104676. https://doi.org/10.1016/j.apgeochem.2020.104676

Hower, J. C., Eble, C. F., Dai, S., & Belkin, H. E. (2016).
Distribution of rare earth elements in eastern Kentucky
coals: Indicators of multiple modes of enrichment? *Inter-
national Journal of Coal Geology, 160–161*, 73–81.

Hower, J. C., Eble, C. F., & Mastalerz, M. (2022). Petrology of
the fire clay coal, bear branch, Perry County, Kentucky.
International Journal of Coal Geology, 249, 103891.

Hower, J. C., Ruppert, L. F., & Eble, C. F. (1999). Lanthanide,
Yttrium, and Zirconium anomalies in the Fire Clay coal
bed, Eastern Kentucky. *International Journal of Coal
Geology, 39*, 141–153.

Jiu, B., Huang, W., Spiro, B., Hao, R., Mu, N., Wen, L., & Hao,
H. (2023). Distribution of Li, Ga, Nb, and REEs in coal as
determined by LA-ICP-MS imaging: A case study from
Jungar coalfield, Ordos Basin, China. *International Jour-
nal of Coal Geology, 267*, 104184.

Karayigit, A. I., Yerin, Ü. O., Oskay, R. G., Bulut, Y., & Córdoba,
P. (2021). Enrichment and distribution of elements in the mid-
dle Miocene coal seams in the Orhaneli coalfield (NW Tur-
key). *International Journal of Coal Geology, 247*, 103854.

Ketris, M. P., & Yudovich, Ya. .E. (2009). Estimations of
Clarkes for carbonaceous biolithes: World average for
trace element contents in black shales and coals. *Interna-
tional Journal of Coal Geology, 78*, 135–148.

Kokowska-Pawłowska, M., & Nowak, J. (2013). Phospho-
rus minerals in tonstein; coal seam 405 at Sośnica-
Makoszowy coal mine, Upper Silesia, southern Poland.
Acta Geologica Polonica, 63, 271–281.

Liu, J., Dai, S., Song, H., Nechaev, V. P., French, D., Spiro, B.
F., Graham, I. T., Hower, J. C., Shao, L., & Zhao, J. (2021).
Geological factors controlling variations in the mineral-
ogical and elemental compositions of Late Permian coals
from the Zhijin-Nayong Coalfield, western Guizhou, China.
International Journal of Coal Geology, 247, 103855.

Lyons, P. C., Spears, D. A., Outerbridge, W. F., Congdon, R.
D., & Evans, H. T. (1994). Euramerican tonsteins: Over-
view, magmatic origin, and depositional-tectonic implica-
tions. *Palaeogeography, Palaeoclimatology, Palaeoecol-
ogy, 106*, 113–134.

Lyons, P. C., Krogh, T. E., Kwok, Y. Y., Davis, D. W., Outerbridge,
W. F., & Evans, H. T., Jr. (2006). Radiometric ages of the Fire
Clay tonstein [Pennsylvanian (Upper Carboniferous), Westphal-
ian, Duckmantian]: A comparison of U-Pb zircon single-crystal
ages and $^{40}Ar/^{39}Ar$ sanidine single-crystal plateau ages. *Inter-
national Journal of Coal Geology, 67*, 259–266.

Lyons, P. C., Outerbridge, W. F., Triplehorn, D. M., Evans, H.
T., Jr., Congdon, R. D., Capiro, M., Hess, J. C., & Nash,
W. P. (1992). An Appalachian isochron: A kaolinized

Carboniferous air-fall volcanic-ash deposit (tonstein). *Geological Society of America Bulletin, 104*, 1515–1527.

Machlus, M. L., Shea, E. K., Hemming, S. R., Ramezani, J., & Rasbury, E. T. (2020). An assessment of sanidine from the Fire Clay tonstein as a Carboniferous ^{40}Ar/^{39}Ar monitor standard and for inter-method comparison to U-Pb zircon geochronology. *Chemical Geology, 539*, art. no. 119485.

Mardon, S. M., & Hower, J. C. (2004). Impact of coal properties on coal combustion by-product quality: Examples from a Kentucky power plant. *International Journal of Coal Geology, 59*, 153–169.

Nechaev, V. P., Dai, S., Chekryzhov, I. Y., Tarasenko, I. A., Zin'kov, A. V., & Moore, T. A. (2022). Origin of the tuff parting and associated enrichments of Zr, REY, redox-sensitive and other elements in the Early Miocene coal of the Siniy Utyes Basin, southwestern Primorye, Russia. *International Journal of Coal Geology, 250*, 103913.

Pédrot, M., Dia, A., & Davranche, M. (2010). Dynamic structure of humic substances: Rare earth elements as a fingerprint. *Journal of Colloid and Interface Science, 345*, 206–213.

Rao, P. D., & Walsh, D. E. (1997). Nature and distribution of phosphorus minerals in Cook Inlet coals, Alaska. *International Journal of Coal Geology, 33*, 19–42.

Rice, C. L., Belkin, H. E., Henry, T. W., Zartman, R. E., & Kunk, M. J. (1994). The Pennsylvanian Fire Clay tonstein of the Appalachian Basin – Its distribution, biostratigraphy, and mineralogy. In: C.L. Rice, ed., Elements of Pennsylvanian Stratigraphy, Central Appalachian Basin. *Geological Society of America Special Paper, 294*, 87–104.

Rietveld, H. M. (1969). A profile refinement method for nuclear and magnetic structures. *Journal of Applied Crystallography, 2*, 65–71.

Robl, T. L, & Bland, A. E. (1977). The distribution of aluminum in shales associated with the major economic coal seams of eastern Kentucky. Proceedings, *Kentucky Coal Refuse Disposal and Utilization Symposium, 3rd*, 97.

Seredin, V. V. (1996). Rare earth element-bearing coals from the Russian Far East deposits. *International Journal of Coal Geology, 30*, 101–129.

Seredin, V. V., & Dai, S. (2012). Coal deposits as potential alternative sources for lanthanides and yttrium. *International Journal of Coal Geology, 94*, 67–93.

Shen, M., Dai, S., Graham, I. T., Nechaev, V. P., French, D., Zhao, F., Shao, L., Liu, S., Zuo, J., Zhao, J., Chen, K., & Xie, X. (2021). Mineralogical and geochemical characteristics of altered volcanic ashes (tonsteins and K-bentonites) from the latest Permian coal-bearing strata of western Guizhou Province, southwestern China. *International Journal of Coal Geology, 237*, 103707.

Spears, D. A. (2012). The origin of tonsteins, an overview, and links with seatearths, fireclays and fragmental clay rocks. *International Journal of Coal Geology., 94*, 22–31.

Sutcu, E. C., Şentürk, S., Kapıcı, K., & Gökçe, N. (2021). Mineral and rare earth element distribution in the Tunçbilek coal seam, Kütahya, Turkey. *International Journal of Coal Geology, 245*, 103820.

Taylor, J. C. (1991). Computer programs for standardless quantitative analysis of minerals using the full diffraction profile. *Powder Diffraction, 6*, 2–9.

Taylor, S. R., & McLennan, S. M. (1985). *The Continental Crust—Its Composition and Evolution* (p. 312). Blackwell Scientific Publishers.

Triplehorn, D. M., & Bohor, B. F. (1981). Altered volcanic ash partings in the C coal, Ferron Sandstone Member of the Mancos Shale, Emery County, Utah. In: US. Geological Survey Open-File Report 81–775, (43 p.).

Vergunov, A. V., Arbuzov, S. I., Soktoev, B. R., Ilenok, S. S., & Chekryzhov, IYu. (2022). Mineralogy and geochemistry of tonstein from coal seam Novy-1A, Kharanor deposit (Zabaykalsky Krai). *Bulletin of the Tomsk Polytechnic University, Geo Assets Engineering, 333*, 15–26.

Ward, C.R., Taylor, J.C., Matulis, C.E., & Dale, L.S., (2001). Quantification of mineral matter in the Argonne Premium coals using interactive Rietveld-based x-ray diffraction. *International Journal of Coal Geology, 46*, 67–82.

Ward, C. R. (2002). Analysis and significance of mineral matter in coal seams. *International Journal of Coal Geology, 50*, 135–168.

Ward, C. R. (2016). Analysis, origin and significance of mineral matter in coal: An updated review. *International Journal of Coal Geology, 165*, 1–27.

Weaver, C. E. (1963). Interpretative value of heavy minerals from bentonites. *Journal of Sedimentary Petrology, 33*, 343–349.

Williams-Jones, A. E., Migdisov, A. A., & Samson, I. M. (2012). Hydrothermal mobilization of the Rare Earth elements – a tale of "Ceria" and "Yttria." *Elements, 8*, 355–360.

Wilson, A. A., Sergeant, G. A., Young, B. R., & Harrison, R. K. (1966). The Rowhurst tonstein, North Staffordshire, and the occurrence of crandallite. *Yorkshire Geological Society Proceedings, 35*, 421–427.

Winchester, J. A., & Floyd, P. A. (1977). Geochemical differentiation of different magma series and their differentiation products using immobile elements. *Chemical Geology, 20*, 325–343.

Zhao, L., Ward, C. R., French, D., & Graham, I. T. (2012). Mineralogy of the volcanic influenced Great Northern coal seam in the Sydney Basin, Australia. *International Journal of Coal Geology, 94*, 94–110.

Zhang, Z., Lv, D., Hower, J. C., Wang, L., Shen, Y., Zhang, A., Xu, J., & Gao, J. (2023). Geochronology, mineralogy, and geochemistry of tonsteins from the Pennsylvanian Taiyuan Formation of the Jungar Coalfield, Ordos Basin, North China. *International Journal of Coal Geology, 267*, 104183.

Zhang, Z., Lv, D., Wang, C., Hower, J. C., Raji, M., Wang, T., Zhang, J., & Yang, Y. (2022). Mineralogical and geochemical characteristics of tonsteins from the Middle Jurassic Yan'an Formation, Ordos Basin, North China. *International Journal of Coal Geology, 253*, 103968.

Ⓐ Springer